UNIVERSITY OF MISKOLC
FACULTY OF MECHANICAL ENGINEERING AND INFORMATICS

LATHE CHATTER PREVENTION BY SPINDLE SYSTEM STRUCTURAL MODIFICATIONS

ISTVÁN SÁLYI DOCTORAL SCHOOL OF MECHANICAL ENGINEERING SCIENCES

DESIGN MACHINES AND STRUCTURES
DYNAMICS AND STABILITY OF MACHINE TOOLS

Head of Doctoral School

Dr. Gabriella Bognár

DSc., Professor

Scientific Supervisors

Dr. Ferenc Sarka
Associate Professor

Dr. Ferenc János Szabó
Associate Professor

Dr. Attila Szilágyi*
Associate Professor

Written by:
Mohammad Jehad Mohammad Alzghoul
IM04C8

Miskolc

2025

Acknowledgments

First and foremost, I express my deepest gratitude to Allah, my God, for granting me the strength, patience, and guidance to complete this journey. Without His blessings, none of this would have been possible.

I am profoundly grateful to my family. My father provided wisdom, guidance, and constant encouragement, serving as a driving force throughout this process. My mother's unconditional love and support were an anchor, inspiring perseverance and determination.

A special acknowledgment goes to my best friend Shereen, who stood by me every step of the way during my time in Hungary. Her unwavering support and encouragement were instrumental in maintaining my progress and motivation.

I would also like to recognize Ahmad Dahesh for his invaluable assistance with complex coding problems. His expertise and willingness to help were crucial in overcoming many challenges during my research.

Finally, I extend sincere appreciation to Professor Brian Stone for generously sharing important codes from his work. His contributions were immensely helpful and significantly aided the progress of my research.

To all who have supported me on this journey, I am deeply thankful.

Supervisor's Recommendation

Alzghoul Mohammad graduated from the University of Miskolc in 2020 as a mechanical engineer. After graduation, he began his PhD studies under the supervision of our colleague Attila Szilágyi PhD. I met the candidate in 2022, after the sudden death of Attila Szilágyi. The topic he brought with him was a bit foreign to my field of expertise, but with my supervisor colleague, Ferenc János Szabó PhD, we did our best ensure that the 1.5 years of work he had begun would not be wasted. We led his topic in a direction, in which we could be a helpful partner of the Candidate

Right from the first semester together, I got to know Mohammad as a very dedicated student blessed with a good technical sense. He always completed his work with great care, attention to details, great accuracy, persistent diligence, and on time. At the beginning of the collaboration he relied on the ideas of the supervisors regarding where the research that had been started could be continued. By the end of the 4 years of study, he had become a researcher who is able to independently provide a solution to a research problem. He is able to recognize the novelty of the results and formulate it appropriately. He is able to process and systematize the research results.

During his doctoral work, he worked on the optimization of the spindle of lathe machines. He approached the optimization from the perspective of what geometry changes could be used to steer the construction in a direction that would help avoid the chatter phenomenon during machining. He carried out his work not only taking into account the design, but also the user's aspects. During the optimization, he also mastered the use of several optimization procedures. At the end of his PhD study, he worked completely alone when formulating the new scientific results achieved, which shows his ability.

During his studies, he prepared 7 scientific publications about his research. Among the publications, several were registered in Scopus and have a Q rating. It is a special merit that he has a publication that is referred in a paper published in a Q1-rated journal.

During our regular consultations, we talked not only about the profession, but also about family, history, politics, and religion. During these conversations, I got to know a kind-hearted and progressive-minded person. The difference between our cultures never caused any problems. His presentation at the departmental discussion on June 25, 2024 received a lot of praise from the participating colleagues and reviewers, both in its content and presentation style. This also predestines the Candidate for active participation in scientific life.

Based on the above, I recommend to the Honoured Review Committee to award the doctoral title to Alzghoul Mohammad.

Miskolc, 29. 04. 2025.

Dr. Ferenc Sarka

associate professor, supervisor

Supervisor's Recommendation

Made by: Ferenc János Szabó, associate professor at Institute of Machine and Product Design

at University of Miskolc, Hungary.

For Mohammad Alzghoul, who is applying for the PhD degree at the University of Miskolc.

Mohammad Alzghoul finished his MSc on CAD- CAM specialization in 2018.

From 2020, he is PhD student at the University of Miskolc, his first supervisor was Attila Szilágyi in the Institute of Machine tools at University of Miskolc. Because Attila Szilágyi deceased, new supervisors from 2022 are Ferenc Sarka and myself (Ferenc János Szabó), at the Institute of Machine and Products Design.

The theme of his doctoral research is Finite element design and optimization of the spindle system of lathes.

The date of the Complex exam is 27. June 2022. Departmental discussion has been made on 25 June 2024. He received the Pre- degree certification on 18 October 2024.

In 2023, he followed the course for PhD students "Multidisciplinary Optimization of Machine Structures", which contains finite element modeling and optimization in ANSYS finite element program system and usage of the grapho- analytical optimization algorithm based on the Kuhn-Tucker optimality criterion.

He published the results of these optimization studies in three publications, which are accepted as Scopus publications, so it is possible to say that he achieved important and interesting results and his research work is efficient.

All along the time of the common research and cooperation, it was a great pleasure for me to work together with him, it was a great success for me to show an effective method to optimize the structure and he quickly understood and apllied it.

On the basis of the above mentioned things I recommend Mohammad Alzghoul for the scientific degree of PhD.

Miskolc, Hungary, the 15th of May, 2025.

Ferenc János Szabó, associate professor

Contents

LIST OF FIGURES

LIST OF TABLES

Nomenclature

$M\ (x,t)$	Bending moment function
$V\ (x,t)$	Shear force function
$f\ (x,t)$	External force per unite length of the beam function
ρ	Mass density of the beam [kg/m^3]
A(x)	Cross-sectional area of the beam [m^2]
w	Vertical deflection [m]
t	Time [s]
E	Young's modulus [N/m^2]
I	Moment of inertia of the beam cross section [m^4]
ϕ	Angle of rotation of the cross-section about the neutral axis due to bending [rad]
G	Shear modulus [N/m^2]
X(x)	Solution related to space [m]
T(t)	Solution related to time [s]
β	Eigenvalue of the beam vibration
μ	Mass attached to the free end of the beam [kg]
$\{\ddot{X}\}$	Acceleration vector [m/s^2]
$\{\dot{X}\}$	Velocity vector [m/s]
$\{X\}$	Displacement vector [m]
$[M]$	Mass matrix [kg]
$[R]$	Damping matrix [N.s/m]
$[K]$	Stiffness matrix [N/m]
$\{F\}$	External load vector [N]
$[R_{gyro}]$	Gyroscopic matrix [Kg. m^2/s]
$[H]$	Circulatory matrix [Kg. m^2/s]
K	Radial stiffness [N/m]
F	Radial load [N]
δ	Radial deformation [mm]
σ	Radial stress [MPa]
A	Applied force area [m^2]
R	Internal radius next to the chuck [mm]
t	Thickness of the shaft [mm]
α_{xx}	Receptance [m/N]
β_{xx}	Receptance of system B [m/N]
γ_{xx}	Receptance of system C [m/N]

ζ	Viscus damping ratio
q	Angular frequency [rad/s]
m_s	Mass of the Shaft [kg]
x_s	Displacement of the shaft [m]
x_h	Displacement of the housing [m]
$a_1 - a_4$	Coefficients of the general solution form $X_1(x)$
$b_1 - b_4$	Coefficients of the general solution form $X_2(x)$

1 INTRODUCTION

Chatter in machining is a common and significant issue that affects various machining processes, such as milling, turning, and drilling. It occurs when the cutting tool and the workpiece interact in an unstable manner, leading to vibrations that can have detrimental effects on the machining operation. Reducing or avoiding chatter represents a significant challenge within the realm of machining dynamics. However, there has been a relatively limited emphasis on addressing chatter by considering the spindle systems in turning. The majority of research efforts have predominantly focused on exploring solutions related to the cutting tool itself.

The primary objective of this research is to optimize a spindle system of a lathe machine specifically with respect to chatter occurrence. This optimization entails implementing structural modifications to the spindle system while ensuring its structural integrity remains unaffected under static loading conditions. By focusing on these modifications, the study aims to enhance the dynamic performance of the spindle system, ultimately mitigating chatter during machining processes.

This chapter serves as an introductory section to the study, encompassing several key aspects. It begins by presenting the background and contextual information relevant to the research. Subsequently, it addresses the research problem and outlines the specific aims, objectives, and questions that guide the study. Additionally, the chapter highlights the significance of the research and acknowledges any limitations associated with the study.

1.1 Background

To establish the relevance of the research, it is essential to highlight the significance of lathe machining and the impact of chatter on its outcomes. Lathe operations play a crucial role in manufacturing processes across various industries, enabling the production of precise and intricate components.

Chatter, a phenomenon in machining, has numerous consequences such as poor surface finish, lack of accuracy, high noise, tool wear, and energy wastage. These undesirable outcomes necessitate the exploration of methods to avoid chatter. Given the wide range of products available in the market, which leads to increased number of machining operations, the probability of chatter occurrence also rises. Therefore, further research on this phenomenon is

imperative to address the challenges posed by increased machining operations and durations, and to minimize the likelihood of chatter. Figure 1 illustrates the trend of publications related to chatter over a span of several years. The x-axis represents the years, while the y-axis represents the number of publications. The chart reveals that there was a gradual increase in publications on chatter from the earlier years to the more recent ones. The number of publications initially started at a lower level and showed a steady rise over time, with a notable spike observed in the later years. The data indicates a growing interest and research focus on the topic of chatter within the academic community throughout the analyzed period [1].

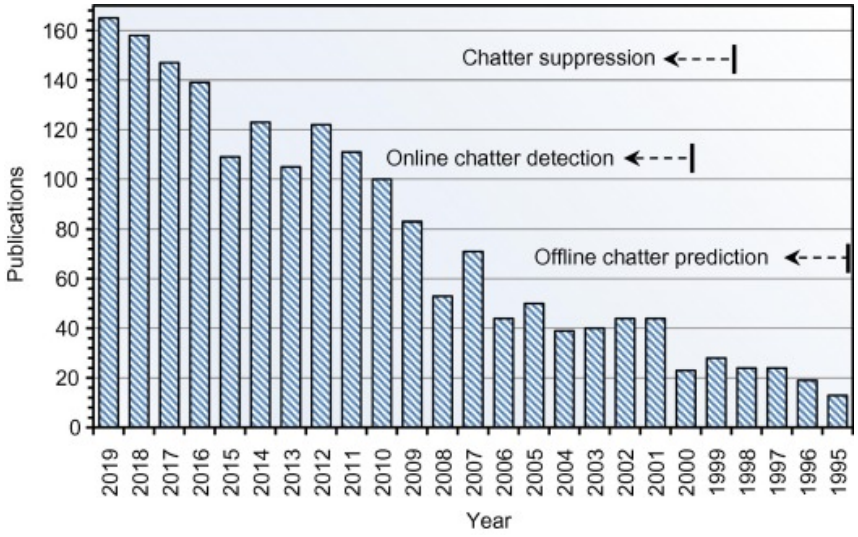

Figure 1. Trend of Chatter Publications Over Time [1].

1.2 Research Problem

Chatter in machining, particularly in turning, has various solutions primarily related to cutting conditions and cutting tools. One example is the utilization of the Spindle Speed Variation (SSV) technique. This technique involves continuously varying the spindle speed during cutting, which effectively keeps the cutting process outside the chatter zone. Chatter is a resonance frequency that necessitates specific conditions for its occurrence, and the spindle speed is one of these critical conditions. By continuously changing the spindle speed within an acceptable range, the likelihood of chatter is effectively eliminated [2]. Another method involves setting the cutting parameters using a Stability Lobes Diagram (SLD), which can be generated through two approaches. The first approach involves experimental methods to construct the SLD, which achieved by carrying out machining operations under different cutting conditions to gather data, from which the stable and non-stable areas are identified. Figure 2 illustrates an experimentally constructed Stability Lobe Diagram (SLD).

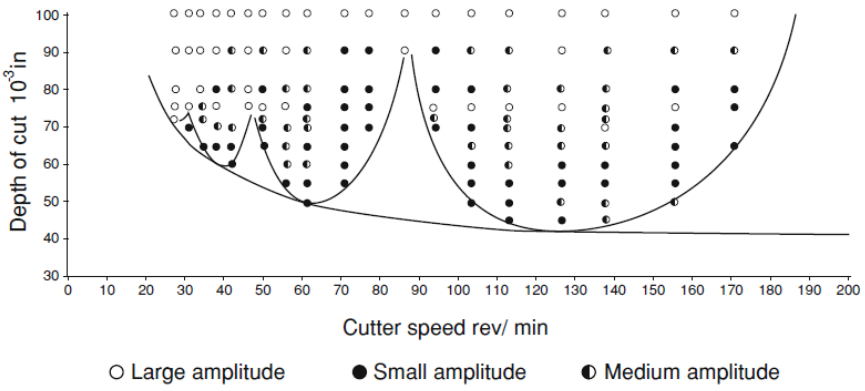

Figure 2. Experimental stability Lobe diagram for milling [3].

The second approach involves theoretical methods utilizing chatter theory. Figure 3 illustrates an example of an SLD constructed using chatter theory.

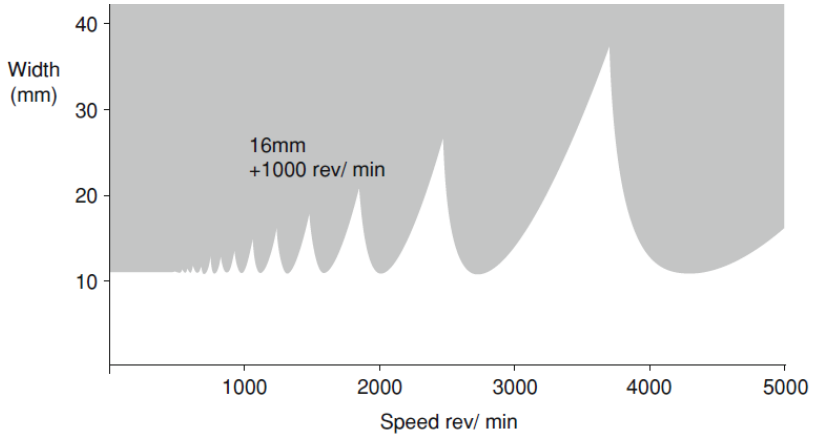

Figure 3. An SLD constructed using chatter theory.

By employing an SLD, machinists can optimize the cutting parameters to ensure stable machining conditions and mitigate the risk of chatter occurrence [3]. Another method involves employing the so-called, Tunned Mass Damper (TMD) tools. The principle behind a TMD cutting tool is to introduce a secondary mass, called the tuned mass, which is precisely tuned to counteract the vibrations generated during cutting. This process does not eliminate the original resonance frequency of the system but mitigates the resonance effect by distributing the energy between the system and the TMD, effectively reducing the peak response of the system at its resonance frequency. The tuned mass damper is strategically positioned and designed to effectively reducing chatter and improving the machining stability of the machining process [4, 5]. Figure 4 illustrates a TMD boring bar.

Figure 4. Buffered impact damper in boring bar [6]

Despite the various solutions proposed to address chatter in turning, less attention has been given to the modification of the spindle system itself, particularly the structural aspects of the spindle system in lathe machines. One area of research that has focused on this aspect is the multi-objective optimization of the machine tool spindle-bearing system. This study aimed to optimize the bearing preload and bearing location within the spindle system. The objective was to enhance the performance of the spindle system in terms of natural frequencies, static stiffness, and total friction torque. By optimizing these parameters, the goal was to achieve improved dynamic stability, enhanced rigidity, and reduced frictional losses within the spindle system, ultimately contributing to a reduction in chatter during turning operations. [7]. Figure 5 illustrates a lathe machine spindle system, showing the main components: a shaft, a chuck, and bearings.

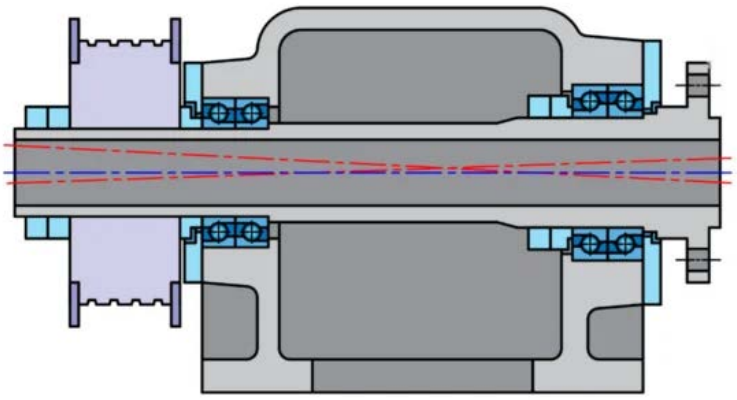

Figure 5. An exemplary schematic drawing of a CNC lathe spindle assembly [8]

In another study, a genetic algorithm was utilized to optimize the bearing locations within a spindle system with the objective of maximizing the first mode natural frequency, through the application of the genetic algorithm. The study sought to achieve an improved spindle system design that would enhance stability and minimize the likelihood of chatter during machining operations [9]. Another study optimized a spindle system in terms of optimum energy efficiency [10]. Considering the limited number of studies focused on optimizing spindle

systems in terms of chatter occurrence, there is a clear need for further research to address this gap.

It is essential to strive for a balanced approach in the field of chatter in turning, addressing both the cutting tool and cutting parameters, as well as the design of the spindle system. By exploring and advancing research in these areas, a comprehensive understanding of chatter in turning can be achieved, leading to more effective strategies for chatter mitigation. This approach will contribute to improving the overall stability and performance of machining processes, enhancing the quality of machined components and reducing the detrimental effects of chatter. Furthermore, incorporating the concept of an optimized spindle system during the design stage introduces an additional layer of consideration in tackling chatter in turning. The significance of this lies in the fact that optimizing the spindle system can be implemented early on, with minimal or no additional cost in assembling the spindle system. Moreover, a well-designed spindle system can possess inherent properties that maximize its performance in resisting chatter. By focusing on the spindle system design, manufacturers can proactively address chatter-related challenges, leading to improved stability and enhanced machining outcomes. This approach not only enhances the effectiveness of chatter control but also contributes to the overall efficiency and productivity of the turning process.

1.3 Research Aim, Objectives and Questions

Considering the limited research on optimizing spindle system design to reduce or avoid chatter in turning, this study aims to address this gap by presenting a case study. The focus is on optimizing a spindle of lathe machine system using two distinct methods to minimize chatter occurrence. Importantly, the study ensures that the structural integrity of the spindle system remains unchanged throughout the optimization process.

The objectives of this research can be summarized as follows:

a. To identify the most suitable theory or method for analysing a lathe machine spindle system.
b. To investigate the impact of altering dimensions such as the dimensions of the shaft of the spindle, rear bearing location on the behaviour of the system.
c. To optimize the spindle system using the RSM (Response Surface Methodology).
d. To optimize the spindle system using the Kuhn-Tucker optimality criterion, employing the Grapho-Analytical technique.

e. To compare the optimization results obtained from the two optimization techniques.

1.4 The Importance of the Research

This research holds significant value in the field of machining and industry by addressing the lack of research on optimizing spindle system design to reduce chatter in turning. It intends to fills a crucial gap in knowledge and provides practical implications that are noteworthy. These implications include improved machining efficiency, cost savings through reduced rework and tool wear, and increased competitiveness through high-quality manufactured parts. By offering valuable insights into different design optimization approaches, the research guides future studies and industry best practices. Disseminating the findings can enhance industry-wide productivity, promote technology transfer, and drive the adoption of optimized spindle systems. This not only benefits manufacturers but also contributes to the advancement of the machining industry as a whole. Furthermore, the research highlights the advantage of having a spindle that encounters resonance only at high levels of excitation frequency, allowing for better cutting conditions, resulting in increased productivity and improved quality of machined parts. One of the advantages of this research is its generalizability, which allows the findings to be applicable to a wide range of industry settings. The dissertation focuses on optimizing spindle system design to reduce chatter in turning, a fundamental issue in machining operations. The principles and methodologies explored in this research can be applied to various machine tools. The generalizability of the research enhances its practical relevance and widens its impact, making it a valuable resource for those seeking to optimize spindle system design and improve machining performance.

1.5 Limitations

One significant limitation of this research lies in the assumptions made during the dissertation. Firstly, the research assumes a constant bearing stiffness, neglecting the fact that the stiffness of the bearing can vary over time due to factors such as its geometry and operational conditions. This variation introduces what is known as parametric excitation, which can affect the dynamics of the spindle system. By assuming a constant stiffness, the research may overlook the influence of this varying stiffness on chatter behaviour and the effectiveness of the optimized spindle system design.

Secondly, the research assumes a fixed size for the workpiece, disregarding the fact that the workpiece can undergo dimensional variations during machining operations. Furthermore, the

volume of the workpiece may also change as machining progresses. While the research acknowledges the importance of investigating the effect of workpiece volume, the assumption of a fixed workpiece size limits the generalizability of the findings to situations where workpieces exhibit significant dimensional and volumetric variations.

These limitations underscore areas where further research and investigation could enhance the understanding and practical application of the research findings. By addressing these assumptions, future studies can provide a more comprehensive and accurate assessment of the behaviour of the spindle system and its optimization for chatter reduction in turning operations.

1.6 The Structural Outline of the Research

Chapter one of the research presents an introduction to the study, providing the necessary context. It outlines the research objectives and identifies the key research questions to be addressed. The chapter also highlights the significance and value of conducting such research in the given field. Furthermore, the limitations of the study are acknowledged and discussed, providing transparency and setting the scope for future improvements and refinements.

Chapter two of the research focuses on conducting an in-depth review of the existing literature in the field of machining chatter, with a specific emphasis on spindle system structural modifications. This literature review aims to explore and analyse the current state of knowledge, theories, and methodologies related to machining chatter and its connection to the modifications made to spindle systems.

Chapter three presents the theoretical framework employed in this research. Two main beam theories are explored to understand their behavior and characteristics.

Chapter four presents a comprehensive analysis of two distinct spindle systems. The first spindle system is examined utilizing the Euler-Bernoulli beam theory, while the second one is analyzed using the Timoshenko beam theory. The impacts of various variables on these spindle systems understood and evaluated through the analysis.

Chapter five shows the analysis to enhance the performance of a lathe spindle system by addressing two key aspects: minimizing chatter occurrence (when the excitation frequency aligns with the natural frequency of spindle) and improving stress capacity. These improvements are pursued while maintaining the same overall mass of the system.

Chapter six sums up the main findings, impacts, and future work from this research on optimizing lathe spindles to reduce chatter. The explored design changes show potential for a better spindle performance through higher natural frequencies.

2 LITERATURE REVIEW

Chatter is a self-excited vibration that takes place during turning operations. It is either to be avoided or reduced for its negative impact on the machine tool, the workpiece surface finish and the cutting tool life. Many research has been carried out in this domain to understand this phenomenon which leads to finding ways to detect, identify, avoid, reduce and control chatter in turning processes. In this chapter, chatter research related to turning processes is reviewed and summarized. The aim of this literature review is to provide a comprehensive overview of chatter in turning, with a particular focus on exploring the research gap related to spindle system structural modifications and their impact on chatter. The review begins by discussing chatter in general, highlighting its causes, effects, and mitigation strategies. It then narrows down the focus to examine the existing literature specifically pertaining to spindle system structural modifications as a mean to control or eliminate chatter. By synthesizing and analysing the relevant studies, this review aims to identify the current state of knowledge, highlight the gaps in research, and provide insights for future investigation in this specific area.

2.1 Introduction

Chatter has four main types: regenerative chatter, mode coupling chatter, frictional chatter [11] and force-thermal chatter [12]. In machining, when chatter is present, the surface quality is poor, the tool life is shorter and the productivity decreases [13]. The earliest work related to chatter was performed by Arnold [14]. He investigated experimentally and analytically the behaviour of a cutting tool during the cutting process of a lathe machine and came up with an explanation about the chatter generation mechanisms. It was shown that chatter is a result of the internal forces generated during the cutting process, not a result of external periodic forces. In the recent years, various methods were suggested to suppress chatter. Yao [15] proposed a method for chatter identification before it is fully developed, based on wavelet and support vector machine. Anderson [16] developed a passive adapter to suppress resonance vibrations of an end mill cutter. Albizuri [17] proposed a method to reduce chatter vibrations using actively controlled piezoelectric actuators. Dohner [18] used the so-called active control approach for mitigating chatter. Chen [19] used active magnetic bearings for the aim of suppression of machining chatter. Studies of Wu [20], Otto [21] and Kambiz [22] use variable spindle speed machining to suppress chatter. Yang [23] used multiple tuned mass dampers to suppress machine tool chatter. Tobias [24] explained that a machine-tool system including the cutting tool, the tool holder and the workpiece witnesses free, forced and self-excited

vibrations. Free and forced vibrations can be detected and suppressed since they are the results of shocks and unbalances respectively. Due to the complex nature of self-excited vibrations in machining processes and due to their harmful effects, they are in interest of research. Chatter that results from the self-excited vibrations is classified into two main categories: primary and secondary chatter [25]. Primary chatter is of less interest as it is the result of mainly the interaction between the cutting tool and the workpiece. When it comes to the secondary chatter as it is the result of the regeneration of the wavy surface on the just machined workpiece surface, it is more in interest of research and investigation. Moreover, compared to the other types of vibrations, this one is the most harmful one [26]. Figure 6. illustrates the difference between chatter occurrence and smooth turning. In this chapter, some of the analytical and experimental techniques for chatter prediction and avoidance are reviewed specifically for turning processes.

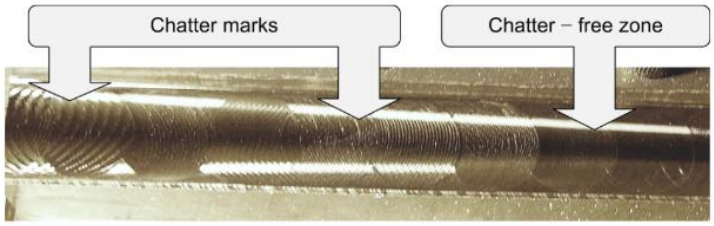

Figure 6. Chatter and chatter-free machining [27].

2.2 Analytical Chatter Prediction Techniques

For the analytical techniques of chatter prediction, a lot of models are available in the literature. The main three ones are the construction of stability lobes diagram (SLD), Nyquist plots and the finite element method (FEM).

2.2.1 Stability Lobes Diagram (SLD)

Stability lobe diagrams are essential tools that are used in optimizing some turning processes parameters for maximizing the rate of material removed while keeping stable cutting conditions. In SLD, the stable and unstable areas are separated by a graph [28] as illustrated in Figure 7. Chatter takes place at high chip widths. For that reason, the depth of cut (chip width) is the most important factor of cutting in terms of chatter presence. The maximum value of depth of cut without having chatter depends on the workpiece material, cutting speed and feed, and on the geometry of the tool [29].

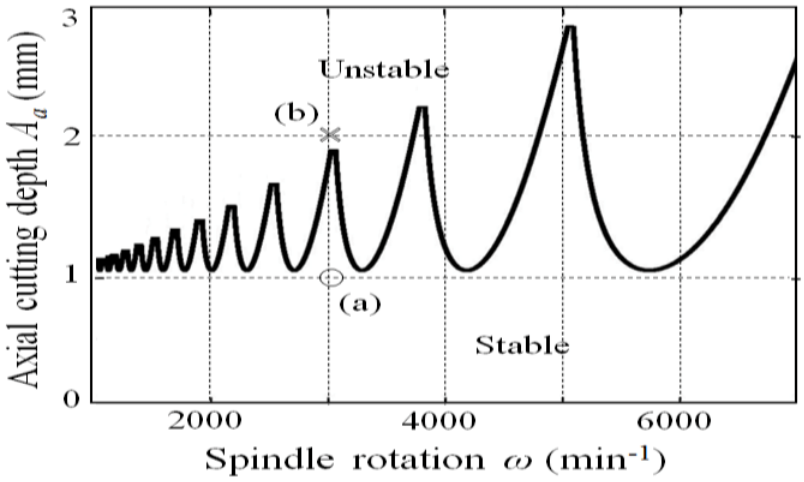

Figure 7. Example stability lobe diagram [30]

Analytical models were presented by many researchers based on the number of degrees of freedom (DoF) of the cutting process. Starting with the single degree of freedom (SDoF) models, Hanna and Tobias [31] introduced a model with a time delay-differential equation. The model takes into consideration the cutting force and the structural stiffness. Chatter is predicted in three categories, unconditionally stable, conditionally stable and unstable which is affected by the width of cut. In this model, even in the stable category there is a presence of unstable periodic motions which is considered a weakness point of the model. Suzuki et al [32] introduced a model defining equivalent transfer function in order to understand the effects of the cutting force ratio and the cross-transfer function on the stability of cutting. An interesting finding is that the critical width of cut in the clockwise and the counterclockwise rotation is different from each other in the experiment. The stability limits were estimated from the vector diagram of the equivalent transfer function. Dombovari et. al [33] analysed large-amplitude motions by introducing a SDoF model that deals with orthogonal cutting. The main equation of the model takes into consideration the non-smoothness when contact between the cutting tool and the workpiece is lost and the regenerative effect of the turning process.

When it comes to the 2DoF models, Chandiramani and Pothala [34] used a 2DoF model of the cutting tool to dealt with the dynamics of chatter. The main finding of that model is that increasing the width of cut results in the occurrence of frequent tool-leaving-cut events and the occurrence of increased chatter amplitudes. Suzuki et al [32] introduced a 2DoF model with the same idea of his SDoF which was mentioned before. It is interesting that both of his models, the SDoF one and the 2DoF one gave the same solution. Chen and Tsao [35, 36] introduced a 2DoF model of a cutting tool with a tailstock supported workpiece and without the tailstock

support using beam theory. The workpiece is treated as a continuous system and under different spindle speeds, the effect of the critical chip width was studied. The strength of this model is that the ability of predicting the stability and evaluating the influence of the elastic deformation and the workpiece natural frequency on the critical chip width for two different workpiece end conditions.

When it comes to the 3DoF models, tool chatter taking into consideration turning dynamics was studied by Dassanayake [37] by employing a 3DoF model at which the workpiece is modelled as a system of three regions, machined, being machined, and unmachined regions connected by a flexible shaft. It was found that for better results, the workpiece vibrations (which are not included in the model) should be considered along with tool vibrations for more accurate results. Eynian and Altintas [38] introduced a 3DoF model of turning by modelling the transfer matrix between the displacements and cutting forces in order to predict the stability regions. Nyquist criterion was used to analytically predict stability regions.

When comparing these analytical models (DoF models), it can be seen that there is no point of going with models that are more than a SDoF unless they result in noticeable higher accuracy. The accuracy of the SDoF models shows quite acceptable results in terms of predicting chatter stability for the turning process. However, it would be a good achievement to have a SDoF model with an enhanced accuracy.

2.2.2 Nyquist Plots

A complex vibration frequency response function can be visualized using Nyquist chart. The dynamic behaviour close to resonances is shown by charting the real and imaginary parts of the response as illustrated in Figure 8. The frequency response function is $G(jw)$ assuming that the response ranges from $-\infty\ to\ +\infty$ and it is given by:

$$G(jw) = H(jw) \tag{2.1}$$

Where $H(jw)$ is the transfer function of the system evaluated on the imaginary axis. $H(jw)$ can be expressed as:

$$H(jw) = \frac{N(jw)}{D(jw)} \tag{2.2}$$

Where $N(jw)$ and $D(jw)$ are polynomials in (jw).

This offers a way to distinguish the modes and provides insight into how they are coupled. Hardware used for frequency analysis frequently incorporates mathematical models like the Nyquist analysis [39].

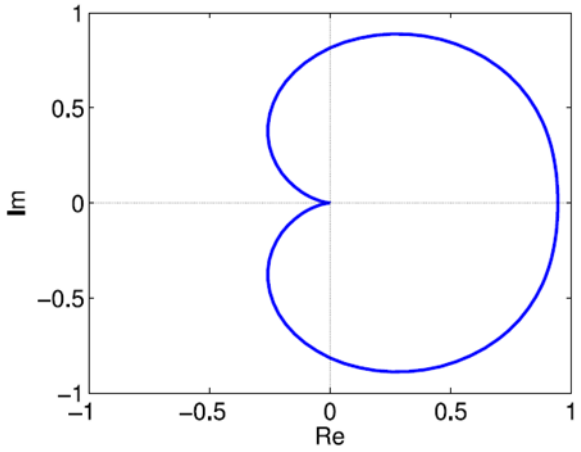

Figure 8. Nyquist plot example [40].

Many researchers used control theory to predict chatter vibrations and they implemented Nyquist plots. By modelling the process using an oriented transfer function using τ decomposition forms, Turkes et al [41] was able to predict chatter vibrations in orthogonal cutting with a SDoF turning system. The stability of the system was investigated using Nyquist criterion in conjunction with an oriented transfer function and a τ decomposition form. Finally, Nyquist technique which is the analytical technique was compared with the time domain simulation technique.

Eynian and Altintas [38] as mentioned earlier, used Nyquist criterion to analytically predict stability regions. Based on the feedback control theory, Merritt [42] proposed a method that uses Nyquist criterion to predict the stability. Using the same concept and based on the feedback control theory as in Merritt [42], Nigm [43] introduced another method that has the benefit of taking the dynamics of the cutting process into consideration. The analysis approach could account for the whole spectrum of regeneration and was robust enough to be implemented either analytically or graphically. Nigm [43] used Nyquist criterion to predict the stability. Instead of plotting the open-loop frequency response locus as required by the Nyquist criterion, the method only requires to plot the operative receptance, since operative receptance is a measure of how the machine tool responds to vibrations during the cutting process. Even faster than plotting the open-loop frequency response locus is plotting the operative receptance. The critical stability parameter was found by Minis et al [44]. It was derived by using the

Nyquist criterion, the criterion was used as an alternative approach by finding the left-most intersection of the Nyquist plot with the negative real axis. Only two-dimensional orthogonal machining could be used with this approach. Also, stability analysis using the Nyquist criterion was performed by Wang and Cleghorn and Altintas et. al [45, 46].

2.2.3 The Finite Element Method

The literature presents a variety of additional methodologies for the improvement of analytical stability analysis. FEM/FEA is one of them. Urbikain et. al [47] created a FE model for the workpiece in ANSYS using 3D 10-node tetrahedral solid elements type SOLID92. A final work piece with 35,516 elements was produced after several geometries were designed and analysed. The modal parameters were then periodically adjusted to include workpiece evolution during machining inside the stability algorithm, which was followed by a FE analysis to create a workpiece. Brecher et al [48] proposed a 3-dimensional turning model based on FEA. This 3D-FEA model has the capability of predicting the cutting forces that will be generated even for complex-shaped tool geometries. Focusing on the thrust and feed forces, a method was employed to shorten the calculation time by employing characteristic diagrams for the computed process forces in the FEA-model. In any production environment, the FEM/FEA approach is very helpful for predicting stability at the design stage of any process, saving time and money. Mahdavine [49] used finite element analysis and ANSYS software to predict the stability of a turning operation. This FEA model takes into account the flexibility of the machine's structure, workpiece, and tool. Baker and Rouch [50] used ANSYS software to build a structural model of the machine tool system and used the FEM approach to investigate the instability of a machining process. However, the validity of the results is not supported by experimental data. Without considering the dynamics of the cutting process models, the impact of structural parameters on machine instability was examined. However, the approach described allows the analysis to take into account the flexibility of both the cutting tool and the workpiece. Airao and Chandrakant [51] used the FEA to analyse a turning process and to understand the effect of temperature, vibration amplitude, frequency and cutting speed on the machining responses.

2.3 Experimental Chatter Prediction Techniques

When it comes to chatter prediction experimental techniques, two main methods have received researchers' attention. The first one is the on-line chatter classification, detection, and monitoring and the second one is the traditional experimental technique for chatter avoidance.

2.3.1 On-Line Chatter Classification, Detection, and Monitoring

In order to minimize or suppress chatter in real-time applications before it completely develops, it is essential to identify it early on. For this reason, it is crucial that CNC controllers and other external devices provide a time-efficient technique for monitoring vibration or/and process signals. For chatter recognition based on pattern recognition, a variety of methods have been employed, such as support vector machines [52], sensor-less methods based on power-factor theory indexes [53], topological data analysis, or the use of regression neural networks when non-linear effects must be addressed [54]. A method for sensor-less chatter detection was presented by Yamato et al. [52]. They achieved this by using two evaluation measures, a mechanical energy factor (MEF) and a mechanical power factor (MPF), both of which are helpful for tracking unstable cutting. The phase difference between the dynamic cutting force and velocity-displacement is shown by these indicators. The authors were able to identify chatter vibration from experimental tests in a precision lathe using only a few calculations [53]. Topological Data Analysis (TDA) and supervised machine learning were integrated by Khasawneh et al. [55] to provide an indicator of impeding presence of chatter. In this method, deterministic and stochastic turning models (with different cutting coefficients) work together. Tansel [56] used a neural network technique to study a three-dimensional turning process. In comparison to traditional time series models, their model demonstrated superior nonlinear effect representation. In addition, precision was improved at higher cutting speeds since there is more space between the lobes. Cherukuri et al. [57] evaluated the behaviour of implementing an artificial neural network (ANN) when it comes to modelling stability in turning. The datasets needed to train the ANN were created using the stability boundaries as a starting point. They discovered that over 90% of the time, the ANN was successful in predicting stability. With the aid of an artificial neural network and a mathematical model of responses based on response surface methodology (RSM), Kumar and Singh [58] analysed the relationship between cutting parameters and chatter degree (ANN). Wavelet Transform was used to eliminate noise from the raw data, and the results demonstrated that ANN was more reliable than RSM. Chatter severity was detected by obtaining a chatter index. Similar methods were employed by Shrivastava et al. [59], who used the wavelet transformation to denoise the raw signal, identify chatter frequency, and calculate chatter index. An operational modal analysis was proposed by Kim and Ahmadi [60] to predict the start of chatter in turning operations. They employed a stability margin of the process, allowing them to predict the start of chatter before the vibrations became intolerable.

In a turning system, the reliability probability of chatter was computed by Liu et al. [61]. They compared their results with a Monte Carlo simulation that presented a modified version of conventional stability lobes, using the first order second moment method (FOSM) and fourth moment method. They coded deeper cuts to cross the stability boundary limitations for the experimental validation. Similar to this, Huang et al. [62] used the Laplace transform to calculate the depth of cut to spindle speed ratio utilizing the Monte Carlo method and advanced first order second moment method. Their predictions were verified by real experiments. With adequate precision, Jimenez Cortadi et al. [63] employed the Linear Mixed Model (LMM) for chatter prediction as well as for wear prediction. A neural network analysis for identifying chatter vibration in turning was carried out by Tian [64]. It was proven that this approach was more effective and reliable than the frequency domain approach.

2.3.2 Experimental Techniques for Chatter Avoidance

When it comes to the experimental techniques for chatter avoidance, it specifically means optimizing the cutting parameters of machining. A time-varying delay can be produced using the spindle speed variation (SSV) approach by distorting chip thickness. As a result, the chatter feedback mechanism is reduced by new, more desirable phase delays between inner and outer chip modulation [65, 66, 67, 68]. There are other approaches to change the rotational speed of the head, but the most effective ones introduce a sinusoidal SSV, in which the spindle speed oscillates sinusoidally at a favourable frequency and amplitude [69, 70].

The method is adaptable to various cutting systems and dynamics. However, when the variation is used, certain previously stable regions of the stability lobe diagram may become unstable. The high spindle accelerations and decelerations, as well as the difficulty in adjusting the frequency and amplitude of the variation, are additional disadvantages of this method. SSV was initially presented in scientific literature to enhance milling processes stability [71]. Al-Regib et al's [72] simple criterion for determining the ideal amplitude ratio was proposed, along with a heuristic criterion to assist in the stability of the process. Based on an energy analysis of the process, Zhang et al. [73] suggested a criterion for determining the ideal SSV amplitude. They also suggested a stability increment index (SII) of SSV in relation to constant spindle speed (CSS). The Ideko-IK4 research team produced various works on the SSV technique used in milling and grinding operations [74, 75]. In some circumstances, such as those involving small workpiece diameters, this approach might be challenging to use. The reference spindle speed, which is limited by the workpiece diameter and work material, is frequently correlated

with the SSV amplitude. High spindle speeds are required for smaller workpiece diameters in order to maintain acceptable cutting speeds. Additionally, the variations in spindle speed cause spindle speeds to increase. In order to allow for a maximum spindle speed, G50 is frequently used while running SSV. The G50 command in CNC programming is used to set a maximum limit on the spindle speed. This is particularly important when running programs that involve SSV to ensure the spindle does not exceed safe operating limits. Also, G96 is used to set a constant surface speed during the machining process. This is especially beneficial when turning operations are performed on a lathe. By keeping the surface speed constant, the machine automatically adjusts the spindle speed as the diameter of the workpiece changes.

A comprehensive formulation for modelling stability in turning and milling operations utilizing SSV for the semi-discretization approach was presented by Insperger et. al in [76]. However, according to some researchers, the SSV approach is more effective in turning than milling since turning naturally involves slower cutting speeds. The stability of the tool analysis was created by Wu et al. [77] utilizing a discrete angle approach. The workpiece's angular position is given by C-axis works as the independent variable in this method. Along with using a stability index criterion, they examined the impact of variable speed machining on the stability of noncircular turning. A closed-loop dynamic model of the noncircular turning process was added by Wu and Chen [78] to the earlier work. They found that both constant and variable spindle speeds led to some improvements in the stability of noncircular turning.

In turning, the most unstable eigenmode was strongly dampened and stabilized, as demonstrated by Yilmaz et al. [79]. An interesting model for the prediction of stability lobes in turning using the SSV approach was proposed by Otto and Radons [80]. They outlined the procedures for putting this technology into practice and noted that, as compared to milling processes, turning processes may achieve greater stable chip widths. Additionally, they suggested advantageous circumstances to regulate the maximum acceleration of spindle speed. The outcomes of the experiments were not included in that research. Adapting the Chebyshev collocation approach and the Homotopy Perturbation Method (HPM) for chatter onset prediction, Urbikain et al. [81] investigated the use of varying turning speeds during the turning of a piece to mitigate this. Speed functions of the sine-wave variety were created and tested for validity using a laser tachometer. Good agreements were reached for chatter types A (Regenerative Chatter which Occurs when the current pass of the cutting tool amplifies the vibrations left from the previous pass) and B (Forced Chatter which is Induced by external

periodic forces acting on the machining process, such as imbalances in the spindle or periodic cutting forces due to tool imperfections). However, they did not take into account temperature effects on spindle speed in their investigation.

It is well known that the stability boundaries depend on a specific spindle speed and uncut chip load combination. Nevertheless, the single time-varying parameters (STVP) approach has demonstrated chatter reduction by, for example, time-varying tool rake angle which instead of having a constant rake angle throughout the machining process, it is dynamically adjusted over time. This adjustment can help in mitigating chatter by constantly altering the cutting conditions, preventing the build-up of consistent vibration patterns, and time-varying feed rate which by varying it, the regeneration cycle of the vibrations is interrupted, reducing the likelihood of resonant conditions that lead to chatter.

However, the Multiple Time-Varying Parameter (MTVP), which in certain circumstances gave chatter reductions up to 80%, can be used to strengthen the resilience of this method, according to the authors [82].

2.4 Literature Related to Spindle Structural Modifications

Literature related to optimizing spindle systems by structural modification is relatively limited compared to other optimization or chatter avoidance methods. In this section, this literature will be reviewed in order to better spot the research gap.

In [83], the author introduces a model aimed at reducing radial vibration in a high precision spindle caused by unbalance force. The study focuses on a flexible rotor supported by angular contact ball bearings, and the equation of motion for the spindle-bearing system is obtained using the finite element method (FEM). Key parameters such as natural frequencies, critical frequencies, and unbalance response amplitudes are determined to analyse the behaviour of the system. To minimize radial vibration, a hybrid genetic algorithm (HGA) is proposed, which takes into consideration factors like **shaft diameter, the damping and the stiffness of the bearings**. Through numerical simulations, it is demonstrated that optimizing the shaft diameter, damping, and stiffness of the bearing leads to a significant reduction in spindle vibration amplitude during operation. Specifically, the results show a satisfactory decrease of approximately 45.1% in radial vibration amplitude at an operating speed of 8000 rpm. This optimization approach significantly improves the accuracy of the machining process.

The main two drawbacks of this study are that the behaviour of the dynamics of the bearings varies over time during the operation of the spindle system, which means, optimizing these parameters can be a good indication about the dynamical performance of that spindle system, but it does not give a very accurate value. The other one is that it does not show how the value of the natural frequency of the first mode is changed after the optimization is carried out.

In [84] the authors focus on the energy consumption and performance optimization of the spindle system in a lathe, which is a significant energy consumer during machine tool operations. Unlike previous methods that primarily targeted improvements in deformation and vibration, this study proposes a comprehensive approach that considers both energy consumption and traditional performance indicators. Initially, an energy consumption function for the spindle is established, and key structural parameters affecting the indicators are selected as decision **variables which are the location of the bearing and the lengths of the shaft segments in addition to the diameter of each shaft segment**. Subsequently, a comprehensive performance objective is determined. To solve the optimization model, a hybrid algorithm is developed. The results demonstrate that the optimized spindle structure successfully reduces energy consumption while maintaining satisfactory static and dynamic performance. The paper systematically analyses the energy consumption and performance characteristics, identifies decision variables, and establishes a structural design optimization model that comprehensively considers energy consumption, static performance, and dynamic performance.

The main drawback of this study is that it does not take into consideration optimizing the mass of the chuck in the optimization problem, giving that the mass of the chuck is a big contributor to the overall mass of the system. As a result, it changes the response of the spindle system in terms of the static and the dynamic performance alongside with the energy consumption of the system.

As in [84], the author of [9] presents a genetic algorithm (GA) optimization approach for determining the optimal locations to install bearings on a motorized spindle shaft in order to maximize its first-mode natural frequency.

In [85], the authors introduce a multi-objective optimization method using particle swarm optimization (PSO) to design a spindle-bearing system. The optimization focuses on improving natural frequencies, static stiffness, and reducing friction torque, with bearing preload and locations as adjustable parameters. Simulation results demonstrate significant enhancements

compared to the initial spindle design, and experimental validation confirms the benefits of the optimized design.

The optimized designs exhibit substantial performance improvements, including increased first and second natural frequencies (10% and 6% respectively) and static stiffness (approximately 26%), as well as reduced friction torque.

The main drawbacks are the computational complexity and the need for further validation in diverse scenarios.

Table 1 provides an overview of different research papers, their objectives in optimizing spindle systems, the variables considered in each study, and any limitations or drawbacks mentioned. It serves as a concise summary of various approaches and challenges in the field of spindle system optimization.

Table 1. Literature related to spindle systems optimization.

Reference	Objective	Variables	Drawbacks
[83]	minimize the spindle vibration amplitude	• Shaft diameter. • Stiffness of the bearings. • Damping of the bearings.	• Variation in bearing dynamics. • Lack of information on natural frequency change
[84]	optimize the energy consumption and performance of a spindle	• bearing locations • diameter of each shaft segment • lengths of the shaft segments	• chuck is not considered in the system
[85]	enhancing the natural frequencies, static stiffness, and reducing friction torque	• bearing preload • bearing locations	• Computational complexity • Further validation is needed

2.5 Conclusion

The first focus of the work was stability prediction using analytical and numerical techniques. As a result, specific sections that highlight the key developments in these techniques (analytical and experimental) are presented. SLDs are the most practical method of chatter vibration process prediction. Even SLDs created using a basic SDoF orthogonal turning model produces results and prediction accuracy that are acceptable. Nyquist plots are a good method when dealing with chatter, still it is in less interest compared to SLDs. The finite element method gives interesting results, yet with the development of the fields with high capabilities, the results are expected to be enhanced. Experimental techniques are an adequate and practical alternative when analytical modelling becomes very complicated and challenging. Finally, as observed from the review, it is evident that insufficient research has been conducted regarding the optimization of the spindle systems through structural modifications. Therefore, the primary focus of this research will be to fill this research gap.

2.6 Related Publication

The majority of the presented literature is published under the title “ANALYTICAL AND EXPERIMENTAL TECHNIQUES FOR CHATTER PREDICTION, SUPPRESSION AND AVOIDANCE IN TURNING: LITERATURE SURVEY”

Design of Machines and Structures, Vol. 12, No. 2 (2022), pp. 31–40. https://doi.org/10.32972/dms.2022.011

3 THEORETICAL FRAMEWORK

The primary objective of this chapter is to present the theoretical frameworks employed in this research, which have been categorized into two groups. The first group pertains to the analysis of the spindle system, wherein two main theories are explored to understand its behavior and characteristics. The second group is concerned with optimization methods, which encompass a range of techniques employed to enhance and optimize the performance of the system under investigation.

3.1 Spindle System Analysis

In the context of spindle systems, it is possible to model them as beam elements due to their structural characteristics. Consequently, two prominent theories are relevant in the analysis of beams: the Euler-Bernoulli Beam Theory, commonly referred to as the classical beam theory [86] or the elementary theory of bending [87], and the Timoshenko Beam Theory. Each theory has distinct advantages and limitations. In the subsequent subsections, a comprehensive review and comparative analysis of both theories will be presented.

3.1.1 The Euler-Bernoulli Beam Theory

The Euler-Bernoulli beam theory is based on three fundamental assumptions [88]:

1. Plane sections of the beam remain planar (as illustrated Figure 9). This assumption holds true when the beam is subjected to pure bending and undergoes negligible shear deformation.
2. Cross sections of the beam remain normal to the neutral axis even after deformation.

The beam cross-section is rigid and can only rotate; the geometry and shape of the cross section do not change significantly.

Experimental measurements have confirmed the validity of the aforementioned assumptions under certain conditions:

- The Euler-Bernoulli beam theory holds true for beams that possess a significant length in comparison to their depth and width. Rao [87] stated, “The thin beam theory is applicable to beams for which the length is much larger than the depth (at least 10 times) and the deflections are small compared to the depth”.

- The material of the beam is assumed to be isotropic and adheres to Hooke's law, which states that stress (σ) is directly proportional to strain (Ɛ) in a linear elastic manner. In other words, the material exhibits linear elasticity with a Young's modulus (E) [88].

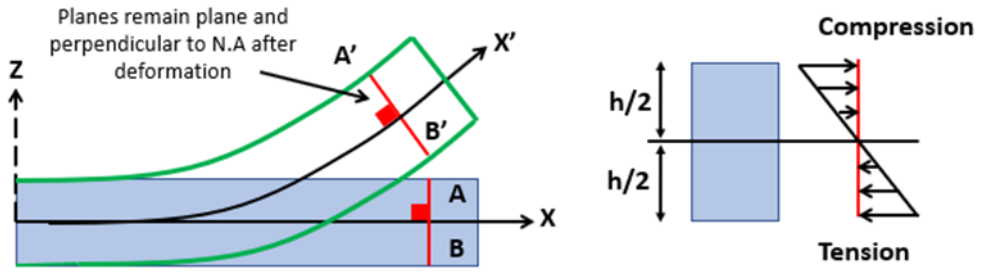

Figure 9. a) Plane and normal section before and after deformation; b) Compression and tension stresses during pure bending.

Considering the free body diagram of the element shown in Figure 10, where the bending moment is M (x, t), the shear force is V (x, t) and f (x, t) is the external force per unite length of the beam and by applying Newton's second law (the force equation of motion in the z direction), then:

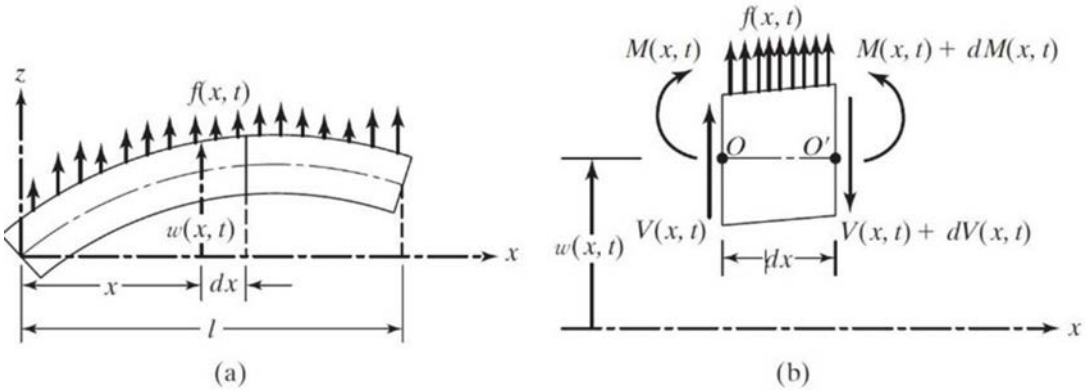

Figure 10. (a) beam in bending, (b) free body diagram of an infinitesimal element [89].

$$-(\boldsymbol{V}+\boldsymbol{dV})+\boldsymbol{f}(\boldsymbol{x},\boldsymbol{t})\boldsymbol{dx}+\boldsymbol{V}=\boldsymbol{\rho A}(\boldsymbol{x})\boldsymbol{dx}\frac{\boldsymbol{\partial^2 w}}{\boldsymbol{\partial t^2}}(\boldsymbol{x},\boldsymbol{t}) \quad \textbf{(3.1)}$$

Without further derivation, the equation of motion of the forced transverse vibration of a nonuniform beam is represented by equation 3.2.

$$\frac{\boldsymbol{\partial^2}}{\boldsymbol{\partial x^2}}\left[\boldsymbol{EI}(\boldsymbol{x})\frac{\boldsymbol{\partial^2 w}}{\boldsymbol{\partial t^2}}(\boldsymbol{x},\boldsymbol{t})\right]+\boldsymbol{\rho A}(\boldsymbol{x})\frac{\boldsymbol{\partial^2 w}}{\boldsymbol{\partial t^2}}(\boldsymbol{x},\boldsymbol{t})=\boldsymbol{f}(\boldsymbol{x},\boldsymbol{t}) \quad \textbf{(3.2)}$$

In brief, The Euler-Bernoulli beam theory eliminates the effect of the shear deformation and the rotary inertia [87, 90]. But real-life structures never meet these assumptions exactly, but usually, approximating them well is enough for the theory to be fairly accurate. So, the theory is said to overestimate the natural frequencies values and underestimate the deflections since it neglects the transverse shear deformation.

3.1.2 Timoshenko Beam Theory

The deformation of elements in the Timoshenko beam theory involves a rotation of the beam cross-section due to bending. It is worth noting that this rotation remains independent of the shear effect in statically determinate beams and in indeterminate beams with full symmetric conditions. However, for beam types other than these, the rotation is influenced by shear stiffness. Consequently, the behavior of the bending moment follows a similar pattern. Therefore, the rotation experienced in Timoshenko beams differs from that observed in Euler-Bernoulli beams.

In addition to the rotation caused by bending, the deformation of such elements also includes an additional angular rotation induced by shear. As a result, the total rotation of the beam cross-section, known as the slope of the deflection curve, is the combined effect of these two rotations. Mathematically, it can be expressed as the summation of these rotations.

Figure 11 illustrates the total rotation of the normal axis, which is the sum of the angular rotation and the rotation that adheres to the Bernoulli-Navier normality hypothesis, where the section remains normal throughout the deformation process [91].

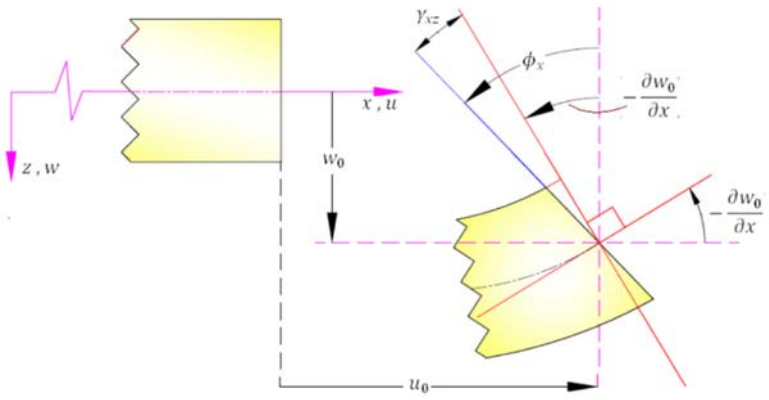

Figure 11. Timoshenko beam cross section deformation [91].

The Timoshenko beam theory, which considers vibrations, can be mathematically represented by a set of coupled linear partial differential Equations (3.3 and 3.4).

$$\rho A \frac{\partial^2 w}{\partial t^2} - f(x,t) = \frac{\partial}{\partial x}\left[kAG\left(\frac{\partial w}{\partial x} - \varphi\right)\right] \quad \textbf{(3.3)}$$

$$\rho I \frac{\partial^2 \varphi}{\partial t^2} = \frac{\partial}{\partial x}\left(EI\frac{\partial \varphi}{\partial x}\right) + kAG\left(\frac{\partial w}{\partial x} - \varphi\right) \quad \textbf{(3.4)}$$

3.1.3 Comparison of the Bernoulli and the Timoshenko Beam Theories

In order to compare and contrast the Euler-Bernoulli beam theory and the Timoshenko beam theory, a table summarizing their key characteristics and differences is provided below. The table highlights the assumptions made, the treatment of shear and rotary inertia, the accuracy of predictions, the applicability, and their common usage. This comparative analysis aims to provide insights into the distinct features and considerations associated with each theory, assisting in the selection of the appropriate beam analysis approach for analyzing the spindle system of the lathe.

Table 2. A Comparative Analysis of Euler-Bernoulli Beam Theory and Timoshenko Beam Theory.

	Euler-Bernoulli Beam Theory	**Timoshenko Beam Theory**
Assumptions	• Plane sections remain planar. • Cross sections remain normal to the neutral axis. • Beam cross-section is rigid and can only rotate	• Cross-sectional planes do not remain planar. • Cross-sectional planes experience shear deformation. • Beam cross-section can undergo significant changes.
Treatment of Shear	Neglected	Considered
Treatment of Rotary Inertia	Neglected	Considered
Accuracy	Overestimates natural frequencies and deflections	Provides better estimations of natural frequencies and deflections
Applicability	Suitable for long and slender beams	Suitable for beams with different geometries and shear effects

In conclusion, after a thorough comparison of the Euler-Bernoulli beam theory and the Timoshenko beam theory, it is evident that the Timoshenko beam theory emerges as the preferred approach for analyzing lathe spindle systems. The table highlights the key advantages of the Timoshenko beam theory, including its consideration of shear deformation, rotary inertia, and the ability to account for different beam geometries. These factors make the Timoshenko beam theory more suitable for accurately predicting the natural frequencies and deflections of lathe spindle systems. Therefore, when analyzing such systems, the Timoshenko beam theory should be prioritized to ensure more accurate results and a better understanding of their dynamic behavior.

4 PROPOSED MODELS AND ANALYSIS

The objective of this chapter is to present a comprehensive analysis of two distinct spindle systems. The first spindle system will be examined, utilizing the Euler-Bernoulli beam theory, while the second one will be analyzed using the Timoshenko beam theory. The first model is simpler than the second one, as the primary objective is to progressively build a spindle system that can be used in the optimization process. The impacts of various variables on these spindle systems will be understood and evaluated through this analysis. By applying these beam theories, insights into the behavior and performance of the spindle under different conditions can be gained, leading to a deeper understanding of the effects of the variables. This scientific approach enables the intricate dynamics of the spindle system to be systematically investigated and comprehended, facilitating potential improvements and optimizations in its design and operation.

4.1 Spindle Model One: Euler-Bernoulli Beam Theory

Beams are considered to be one of the most important and primary components in rotor dynamics, particularly in machine tools. They are highly useful for modeling, simplifying, and analyzing machine tools. The objective of this research is to perform dynamic simulations on a simply supported Euler-Bernoulli beam with an overhang mass. The aim is to derive a general expression that can be used to calculate the natural frequencies and plot the mode shapes of such a system with various configurations, including different beam lengths, second support locations, and overhang mass (which represents the mass of the chuck of a spindle system) values. This beam system is commonly found in many applications of machine tools. The expression is derived using the Euler-Bernoulli beam theory and Newton's second law, and its validity is verified through finite element analysis.

Figure 12 illustrates a pinned-pinned-free beam with an overhang with a mass m attached to the free end of the beam. The beam is assumed to be slender and subjected to a transverse load w.

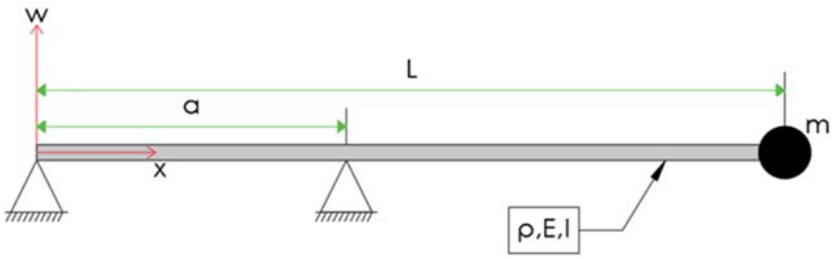

Figure 12. Pinned-Pinned-Free beam with a mass attached to the free end.

Since the interest of this research is about uniform beams and for free vibrations and using Euler-Bernoulli's beam theory the governing equation can be rewritten as:

$$EI\frac{\partial^4 w}{\partial x^4}(x,t) + \rho A\frac{\partial^2 w}{\partial t^2}(x,t) = 0 \tag{4.1}$$

Assuming a solution of Equation (4.1) by the help of the separation of variables method, the solution takes the following form:

$$w(x,t) = X(x)T(t) \tag{4.2}$$

The "X" solution can be written as:

$$(x) = \begin{cases} X_1(x), & 0 \le x \le a \\ X_2(x), & a \le x \le L \end{cases} \tag{4.3}$$

The following flow chart shows the procedure to calculate the beam vibration eigenvalues which are required to calculate the beam natural frequencies.

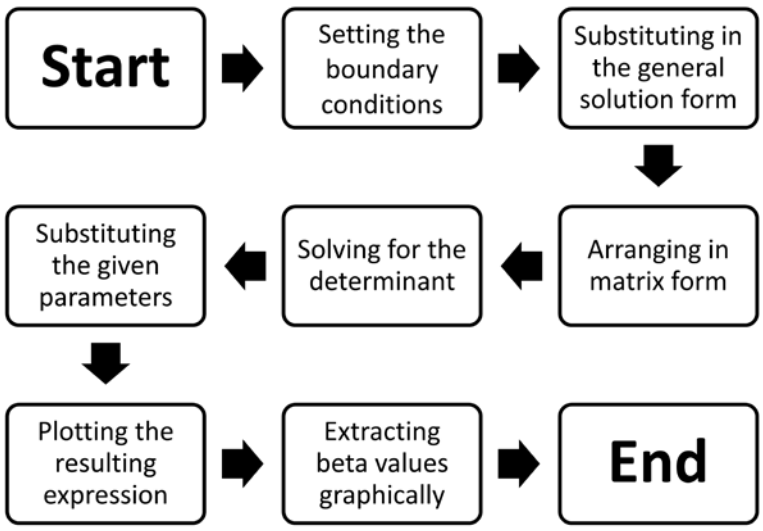

Figure 13. Eigenvalues calculating procedure.

For the presented beam system at Figure 12, the boundary conditions are to be determined at the first pin support, the second pin support and at the free end from left to right. For the first pin, the displacement and the moment are equal to zero, so:

$$\boldsymbol{X_1(0) = 0} \tag{4.4}$$

$$\boldsymbol{\frac{d^2X_1(0)}{dx^2} = 0} \tag{4.5}$$

At the free end, the bending moment is equal to zero and the shear vanishes [92], so:

$$\boldsymbol{\frac{d^2X_2(0)}{dx^2} = 0} \tag{4.6}$$

$$\boldsymbol{I\frac{d^3X_2(L)}{dx^3} - \mu\frac{d^2T_2(L,t)}{dt^2} = 0} \tag{4.7}$$

At the second pin support, the following conditions are present:

$$\boldsymbol{X_1(a) = 0} \tag{4.8}$$

$$\boldsymbol{X_2(a) = 0} \tag{4.9}$$

$$\boldsymbol{\frac{dX_1(a)}{dx} = \frac{dX_2(a)}{dx}} \tag{4.10}$$

$$\boldsymbol{\frac{d^2X_1(a)}{dx^2} = \frac{d^2X_2(a)}{dx^2}} \tag{4.11}$$

After substituting in the general form and arranging in matrix form gives the following matrix:

$$\begin{bmatrix} 0 & 1 & 0 & 1 & 0 & 0 & 0 & 0 \\ 0 & -1 & 0 & 1 & 0 & 0 & 0 & 0 \\ 0 & 0 & 0 & 0 & -\sin(\beta L) & -\cos(\beta L) & \sinh(\beta L) & \cosh(\beta L) \\ 0 & 0 & 0 & 0 & -\cos(\beta L)+\frac{\mu}{\rho A}\beta\sin(\beta L) & \sin(\beta L)+\frac{\mu}{\rho A}\beta\cos(\beta L) & \cosh(\beta L)+\frac{\mu}{\rho A}\beta\sinh(\beta L) & \sinh(\beta L)+\frac{\mu}{\rho A}\beta\cosh(\beta L) \\ \sin(\beta a) & \cos(\beta a) & \sin(\beta a) & \cosh(\beta a) & 0 & 0 & 0 & 0 \\ 0 & 0 & 0 & 0 & \sin(\beta a) & \cos(\beta a) & \sinh(\beta a) & \cosh(\beta a) \\ \cos(\beta a) & -\sin(\beta a) & \cosh(\beta a) & \sinh(\beta a) & -\cos(\beta a) & \sin(\beta a) & -\cosh(\beta a) & -\sinh(\beta a) \\ -\sin(\beta a) & -\cos(\beta a) & \sinh(\beta a) & \cosh(\beta a) & \sin(\beta a) & \cos(\beta a) & -\sinh(\beta a) & -\cosh(\beta a) \end{bmatrix} \begin{bmatrix} a_1 \\ a_2 \\ a_3 \\ a_4 \\ b_1 \\ b_2 \\ b_3 \\ b_4 \end{bmatrix} = \begin{bmatrix} 0 \\ 0 \\ 0 \\ 0 \\ 0 \\ 0 \\ 0 \\ 0 \end{bmatrix} \tag{4.12}$$

Solving for the determinant using Maple software, leads to the transcendental equation as follows:

$$\frac{1\rho A}{7}\Big(\Big((-28\,A\,\rho\,cosh(\beta a)^2 - 28\,A\,\rho\,cos(\beta a)^2 + 56\,\mu\,\beta\,sinh\,(\beta a)\,cosh\,(\beta a) - 56\,\mu\,\beta\,sin\,(\beta a)\,cosh\,(\beta a) + 56\;\rho\,A)sinh\,(\beta L) + 24\,\mu\,\beta\,cosh\,(\beta L)\,sinh\,(\beta a)\sin(\beta a) - 28\cos(\beta L)\,(A\,\rho\cosh(\beta a)\sinh(\beta a) - A\rho\cos(\beta a)\sin(\beta a) + 2\,\mu\,\beta\,cos(\beta a)^2 - 2\,\mu\,\beta)\Big)\sinh\,(\beta L) + 28\Big(A\,\rho\,cosh\,(\beta a)sinh(\beta a) - A\,\rho\,cos(\beta a)\sin(\beta a) - \frac{8\;\mu\,\beta\cosh(\beta a)^2}{7} + \frac{8\;\mu\,\beta}{7}\Big)\cosh(\beta L)\sin(\beta L) + 28\,A\Big((\cosh(\beta a)^2\;cos(\beta L) - \cos(\beta a)^2\cos(\beta L))\cosh(\beta L) + 2\sinh\;(\beta a)\sin\;(\beta a))\,\rho\Big) = 0 \qquad \textbf{(4.13)}$$

Equation (4.13) can be solved to obtain the values of β since the values of ρ, a, A and μ are known for any beam system as shown in the coming section.

After obtaining the values of β from Equation (4.13), the natural frequencies are calculated by Equation (4.14) [93].

$$f_n = \frac{\beta^2}{2\pi}\sqrt{\frac{EI}{\rho A}}\,[Hz] \qquad \textbf{(4.14)}$$

4.1.1 The Verification Model

In this section, a beam model with specific properties is analyzed using the analysis method in the previous sections to obtain the values of the natural frequencies for the first four eigenvalues and the first four mode shapes.

Table 3. The parameters of the validation model.

Parameter	Value
L	1 m
ρ	7850 kg/m^3
E	2.05e+11 N/m^2
μ	0.628 kg
I	1.333 10^{-8} m^4
A	4e-4 m^2
a	0.3 m

Since Equation (4.13) has infinite number of zeros and that the interest of this research is the first four modes, the parameters in Table 3 are substituted in Equation (4.13) and then it is plotted for a range of 4 π domain as follows:

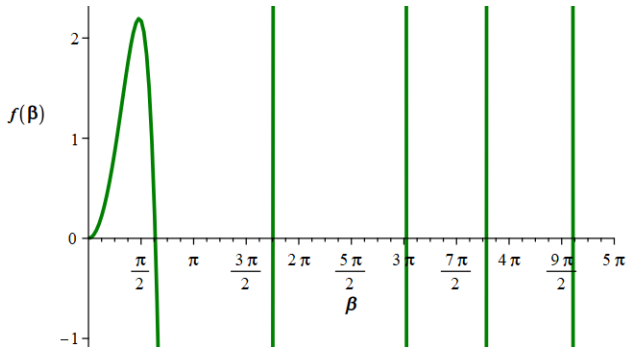

Figure 14. Beta values plot.

Then the zeros of the plot are extracted and substituted in Equation (4.14) to give the natural frequency values as listed in Table 4.

Table 4. Extracted Beta values and calculated natural frequencies.

Beta	Value	$f_n\ [Hz]$
1	1.99	18.72
2	5.52	143.25
3	9.53	426.33
4	11.85	659.5

In order to obtain the Beta values for different second pin support location, instead of repeating the previous step, a figure for calculating Beta values can be obtained from Equation (4.13). For doing so, two variables are defined as follows, $\delta = \beta . l$ and $\lambda = a/l$. After rearranging and substituting them in Equation (4.13) then plotting the new expression for δ and λ yields to Figure 15 as shown below. The curves in the plot correspond to the modes one to four from bottom to up respectively.

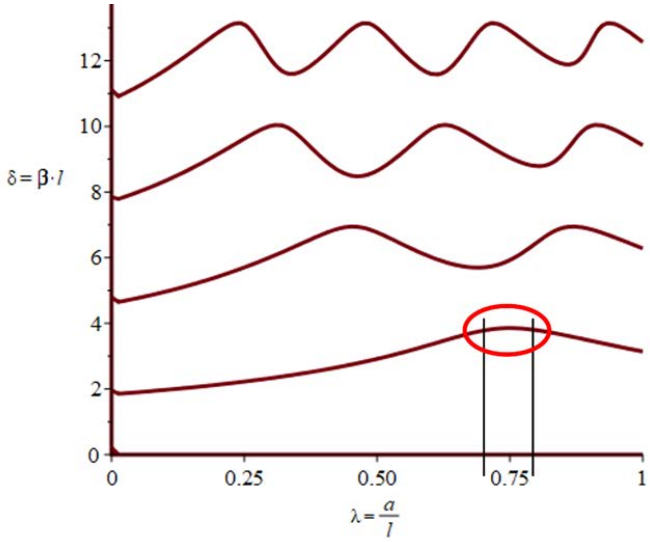

Figure 15. Eigenvalues for first 4 mode.

Figure 15 predicts the highest first natural frequency value to be near the a/l ratio of 0.75. To confirm this result, the following a/l ratios are analyzed to validate the model by FEM.

Table 5. Frequency values.

a/l **Ratio**	**Frequency** $[Hz]$
0.1	13.9
0.2	16.1
0.3	18.8
0.4	22.6
0.5	27.9
0.6	35.8
0.7	47.3
0.8	58.4
0.9	55.2

As can be observed in Table 5, when the support is placed at the opposite end of the mass, the first natural frequency value is the lowest. As the a/lratio increases, the first natural frequency value increases until the a/lratio reaches 0.8. Beyond this point, the first natural frequency value decreases, confirming the findings from Figure 15.

For the mode shapes, the boundary conditions equations are used in order to obtain relationships between the coefficients $a_1, a_2, a_3, a_4, b_1, b_2, b_3\ and\ b_4$ which are the coefficients of the boundary conditions equations (Equations (4.4) to (4.11)). Since there are

no enough equations to obtain the values of the coefficients, the obtained values will be normalized by dividing all the coefficients on b_4.

Substituting the obtained coefficient values in Equation (4.3) and then plotting for each β value, the mode shapes are illustrated in the figure below. The x axis represents the position along the beam system in meter and the y axis represents the normalized displacement.

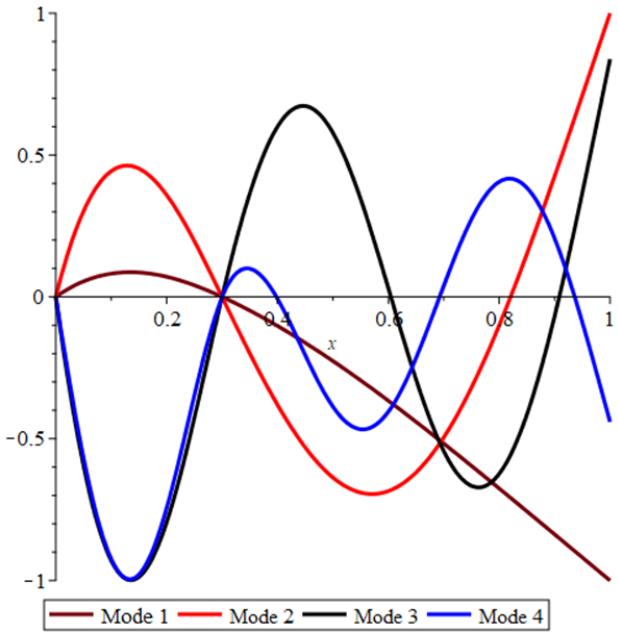

Figure 16. Proposed model mode shapes.

4.1.2 Conclusion

A beam with pinned-pinned-free (Pin support at the start of the beam, then another pin support before the other end of the beam, then a free end of the beam) with a mass attached to the free end is studied. Euler-Bernoulli beam theory is used to derive the transcendental equation which can be applied for different pin support locations that is located between the first pin support and the free end of the beam and for different attached mass values. The eigenvalues for calculating the natural frequencies and the mode shapes were obtained for a validation model.

The developed analytical model can be helpful in design in many engineering applications like cranes arms, machine tools spindles or even machine tools boring bars.

4.1.3 Related Publications

Alzghoul, M., Cabezas, S., & Szilágyi, A. (2022). Dynamic modeling of a simply supported beam with an overhang mass, POLLACK PERIODICA, 17(2), 42-47.
doi: https://doi.org/10.1556/606.2022.00523

4.2 Spindle Model Two: Timoshenko Beam Theory

The goal of this section is to dynamically simulate a turning-center main spindle system utilizing Timoshenko beam theory, employing the systems receptance coupling technique to determine the spindle first three resonant frequencies in the event of transverse vibrations. The findings are then confirmed using the finite element technique using ANSYS software. The significance of analyzing the spindle system described in this study is that it can be utilized to optimize the spindle system in terms of resonance frequencies for improved performance in terms of spindle vibration while the turning center is in operation.

Spindle models are introduced to facilitate more precise dynamical evaluations, ranging from spindle models assume having rigid bearings [94] to models assume having flexible bearings [95] offering a much clearer view of the behavior of this critical part of a turning-center.

4.2.1 Mathematical Modeling Principle

For the spindle system considered, the following assumption are considered:

- the bearings are attached to a rigid frame, which implies that the rest of the machine structure is also ideally rigid.
- The flexural (transverse) vibration of the spindle will also be assumed to be in a single plane, meaning that the movement is restricted to one specific direction perpendicular to the spindle's axis.

The spindle may be broken down into several subsystems, such as shaft components and bearings, which can then be reassembled to form the entire spindle, as illustrated in Figure 17.

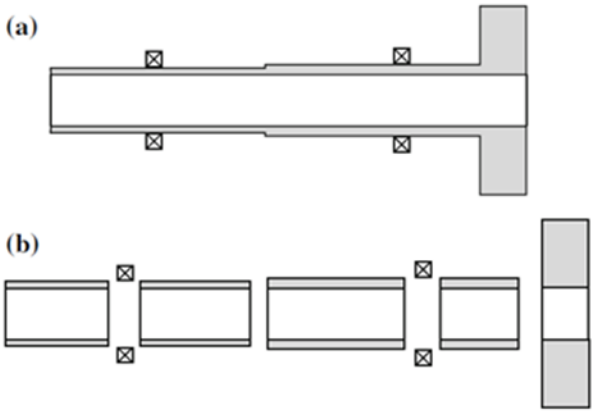

Figure 17. Typical spindle (a), subsystem component (b) [3].

Enforcing equilibrium and compatibility criteria at the joints is a part of the addition of the subsystems process. There are two coupling connections between each subsystem because the connected ends of each coupled ends of subsystem ends must have compatible displacement and slope due to bending for the transverse bending vibration of shafts.

4.2.2 Receptance Definition and Systems Addition

Receptance coupling theory makes the analysis of vibrational energy flows in structures straightforward by treating them as conglomerates of subsystems. It diverges from traditional sub-structuring methods by employing matrices derived from evaluations of substructures' uncoupled modes to assess displacement effects from external and boundary forces. This methodology takes into account variations in substructure damping and estimates the vibrational energy levels of substructures by balancing input and dissipated energies against transfers through coupling nodes.

The approach integrates subsystems, blending the dynamic behaviors of substructures to predict the system's overall displacement response. It is based on the concept of dynamic compliance of structures to external forces, allowing for the modeling of subsystem interactions at coupling points through matrices. This facilitates efficient and direct system modeling, especially useful in scenarios requiring extensive numerical analysis, such as Finite Element Analysis (FEA). It aids in designing structures for optimal performance with minimal vibrational issues and in predicting how changes in a subsystem can influence the vibrational characteristics and energy distribution throughout the system.

Receptances are used in systems approach, the receptance is defined as:

$$\boldsymbol{\alpha_{12} = \frac{X_1 e^{i\omega t}}{F_2 e^{i\omega t}} = \frac{X_1}{F_2}} \qquad \textbf{(4.15)}$$

Where X_1 is the steady-state displacement response of a system at the position and in the direction specified by the subscript 1 and is oftenly a complex number that indicates a phase with respect to the steady exciting force $F_2 e^{i\omega t}$ that is applied to the system at the position and in the direction specified by the subscript 2. The receptance of shafts including shear and rotary inertia effects were derived by Potter and Stone [96] and Stone [97]. Also, the receptance of bearings was derived taking into consideration their stiffness.

For adding systems, the process consists of breaking the combined system A into its component systems, or subsystems B and C, and applying forces to each subsystem at coordinate 1, causing

the separate systems to behave exactly as they would when they were combined as illustrated in Figure 18.

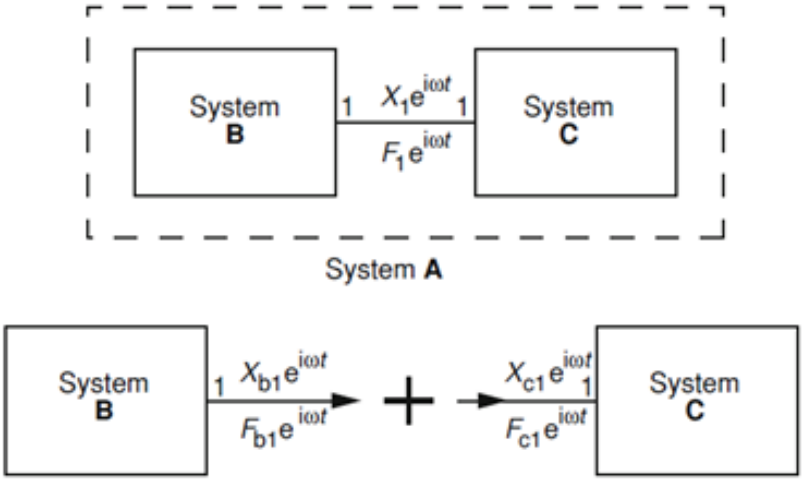

Figure 18. The addition of two subsystems [3].

4.2.3 The Validation Model

After deriving the receptance of all the required components of a spindle system, the spindle system illustrated in Figure 19. is analyzed using systems receptance coupling approach. The shaft elements and the chuck are modelled as hollowed circular sections while the workpiece is modelled as a cylinder.

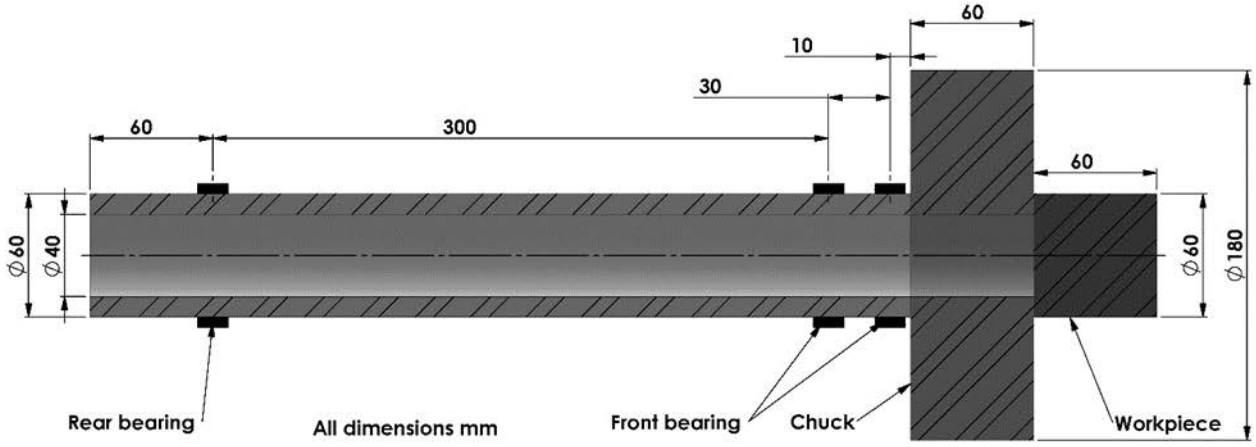

Figure 19. The spindle system including the subsystems and the related dimensions.

Figure 20. illustrates the block diagram of the spindle system including the shaft segments, the bearings, the chuck, and the workpiece. Symbols B, D and F represent the bearings, H represents the chuck, Symbol I represents the workpiece and the rest of the subsystems

represent the shaft segments. The used material of the spindle is assumed to be ASTM A36 steel. The stiffness of the bearing used in the analysis is 7.5x10^8 N/m [3].

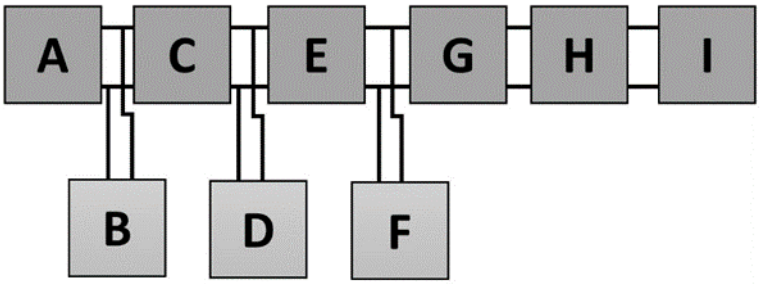

Figure 20. Addition of shaft and bearing subsystems.

For shaft segments, chuck and workpiece (subsystems A, C, E G, H and I respectively), the receptance can be calculated employing the following formulas:

$$\alpha_{OO} = \alpha_{LL} = \frac{F_4\left(\frac{s\zeta^2}{r\eta} - \zeta\right) - F_5\left(\frac{r\eta^2}{s\zeta} - \eta\right)}{\Delta} \tag{4.16}$$

$$\alpha_{LO} = \alpha_{OL} = \frac{\sinh \eta L\left(\eta - \frac{r\eta^2}{s\zeta}\right) + \sin \zeta L\left(\frac{s\zeta^2}{r\eta} - \zeta\right)}{\Delta} \tag{4.17}$$

$$\alpha_{LL'} = \alpha_{L'L} = -\alpha_{O'O} = -\alpha_{OO'} = \frac{F_1\left(\frac{s\zeta^2}{\eta} - \frac{r\eta^2}{\zeta}\right) + F_3(s\zeta - r\eta)}{\Delta} \tag{4.18}$$

$$\alpha_{O'L} = \alpha_{LO'} = -\alpha_{OL'} = \alpha_{L'O} = \frac{F_6(r\eta - s\zeta)}{\Delta} \tag{4.19}$$

$$\alpha_{O'O'} = \alpha_{L'L'} = \frac{F_4\left(sr\eta - \frac{r^2\eta^2}{\zeta}\right) + F_5\left(rs\zeta - \frac{s^2\zeta^2}{\eta}\right)}{\Delta} \tag{4.20}$$

$$\alpha_{O'L'} = \alpha_{L'O'} = \frac{\sinh \eta L\left(sr\eta - \frac{s^2\zeta^2}{\eta}\right) + \sin \zeta L\left(rs\eta - \frac{r^2\eta^2}{\zeta}\right)}{\Delta} \tag{4.21}$$

The quantities η, ζ, s, r, $F_1, F_2, F_3, F_4, F_5, F_6$ and Δ are defined in appendix B. The next step is to calculate the receptance of the bearings

Bearing static stiffness is defined as follows:

$$K_T = \frac{-m_s \ddot{x}_s}{x_r} \tag{4.22}$$

$$x_r = x_s - x_h \tag{4.23}$$

$$\ddot{x}_r = -q x_r \tag{4.24}$$

$$\ddot{x}_s = \ddot{x}_h - q^2 x_r \tag{4.25}$$

$$K_T = m_s\left(q^2 - \frac{\ddot{x}_h}{x_r}\right) \tag{4.26}$$

It should be noted that the stiffness of the bearing has two components, real which corresponds to the static stiffens of the bearing, and imaginary which corresponds to the damping effect.

$$K_T = K_{real} + iK_{imaginary}$$

For the imaginary part, the damping force is assumed to be $iqcXe^{iwt}$, h is defined as qc.
Also, for the viscous damping ratio, it can be expressed as:

$$\zeta = \frac{c}{2\sqrt{km}} \tag{2.27}$$

Also, the damping ratio is:

$$\alpha = \frac{h}{k} \tag{2.28}$$

Then:

$$k + ih = k\left(1 + i\frac{h}{k}\right) = k(1 + i\alpha) \tag{2.29}$$

For subsystems addition, the notations in figure 21 are used.

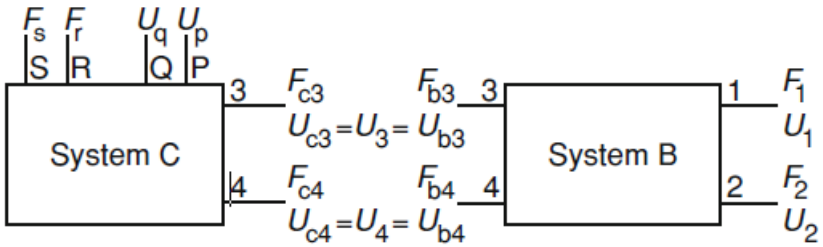

Figure 21. Addition of two subsystems [3]

The two systems are assumed to be separated at coordinates 3 and 4. Also, they vibrate in the same way since they are assumed to be constrained to each other. This constraining of the two subsystems is achieved by forces and moments to be applied at the joining coordinates. F in Figure 21 represents forces or moments, U represents displacements or slopes.

For system B.

$$\begin{bmatrix} U_1 \\ U_2 \end{bmatrix} = \begin{bmatrix} \beta_{11} & \beta_{12} \\ \beta_{12} & \beta_{22} \end{bmatrix} \begin{bmatrix} F_1 \\ F_2 \end{bmatrix} + \begin{bmatrix} \beta_{13} & \beta_{14} \\ \beta_{23} & \beta_{24} \end{bmatrix} \begin{bmatrix} F_{b3} \\ F_{b4} \end{bmatrix} \tag{2.30}$$

$$\begin{bmatrix} U_{b3} \\ U_{b4} \end{bmatrix} = \begin{bmatrix} \beta_{13} & \beta_{23} \\ \beta_{14} & \beta_{24} \end{bmatrix} \begin{bmatrix} F_1 \\ F_2 \end{bmatrix} + \begin{bmatrix} \beta_{33} & \beta_{34} \\ \beta_{34} & \beta_{44} \end{bmatrix} \begin{bmatrix} F_{b3} \\ F_{b4} \end{bmatrix} \tag{2.31}$$

For system C.

$$\begin{bmatrix} U_{c3} \\ U_{c4} \end{bmatrix} = \begin{bmatrix} \gamma_{33} & \gamma_{34} \\ \gamma_{34} & \gamma_{44} \end{bmatrix} \begin{bmatrix} F_{c3} \\ F_{c4} \end{bmatrix} + \begin{bmatrix} \gamma_{3r} & \gamma_{3s} \\ \gamma_{4r} & \gamma_{4s} \end{bmatrix} \begin{bmatrix} F_r \\ F_s \end{bmatrix} \tag{2.32}$$

$$\begin{bmatrix} U_p \\ U_q \end{bmatrix} = \begin{bmatrix} \gamma_{3p} & \gamma_{4p} \\ \gamma_{3q} & \gamma_{4q} \end{bmatrix} \begin{bmatrix} F_{c3} \\ F_{c4} \end{bmatrix} + \begin{bmatrix} \gamma_{pr} & \gamma_{ps} \\ \gamma_{qr} & \gamma_{qs} \end{bmatrix} \begin{bmatrix} F_r \\ F_s \end{bmatrix} \tag{2.33}$$

Employing that $U_3 = U_{b3} = U_{c3}$, $U_4 = U_{b4} = U_{c3}$, $F_{b3} + F_{c3} = F_3$ and $F_{b4} + F_{c4} = F_4$, then:

$$\begin{bmatrix} \beta_{13} & \beta_{23} \\ \beta_{14} & \beta_{24} \end{bmatrix} \begin{bmatrix} F_1 \\ F_2 \end{bmatrix} + \begin{bmatrix} \beta_{33} & \beta_{34} \\ \beta_{34} & \beta_{44} \end{bmatrix} \begin{bmatrix} F_{b3} \\ F_{b4} \end{bmatrix} = \begin{bmatrix} \gamma_{33} & \gamma_{34} \\ \gamma_{34} & \gamma_{44} \end{bmatrix} \begin{bmatrix} F_{c3} \\ F_{c4} \end{bmatrix} + \begin{bmatrix} \gamma_{3r} & \gamma_{3s} \\ \gamma_{4r} & \gamma_{4s} \end{bmatrix} \begin{bmatrix} F_r \\ F_s \end{bmatrix} \tag{2.34}$$

When:

$$\Delta = \begin{bmatrix} \beta_{33} + \gamma_{33} & \beta_{34} + \gamma_{34} \\ \beta_{34} + \gamma_{34} & \beta_{44} + \gamma_{44} \end{bmatrix} \tag{2.35}$$

Then:

$$\begin{bmatrix} F_{b3} \\ F_{b4} \end{bmatrix} = -\Delta^{-1} \begin{vmatrix} \beta_{13} & \beta_{23} \\ \beta_{14} & \beta_{24} \end{vmatrix} \begin{vmatrix} F_1 \\ F_2 \end{vmatrix} + \Delta^{-1} \begin{vmatrix} \gamma_{33} & \gamma_{34} \\ \gamma_{34} & \gamma_{44} \end{vmatrix} \begin{vmatrix} F_3 \\ F_4 \end{vmatrix} + \Delta^{-1} \begin{vmatrix} \gamma_{3r} & \gamma_{3s} \\ \gamma_{4r} & \gamma_{4s} \end{vmatrix} \begin{vmatrix} F_r \\ F_s \end{vmatrix} \tag{2.36}$$

$$\begin{bmatrix} U_1 \\ U_2 \end{bmatrix} = \begin{vmatrix} \beta_{11} & \beta_{12} \\ \beta_{12} & \beta_{22} \end{vmatrix} \begin{vmatrix} F_1 \\ F_2 \end{vmatrix} - \begin{vmatrix} \beta_{13} & \beta_{14} \\ \beta_{23} & \beta_{24} \end{vmatrix} \Delta^{-1} \begin{vmatrix} \beta_{13} & \beta_{23} \\ \beta_{14} & \beta_{24} \end{vmatrix} \begin{vmatrix} F_1 \\ F_2 \end{vmatrix} + \begin{vmatrix} \beta_{13} & \beta_{14} \\ \beta_{23} & \beta_{24} \end{vmatrix} \Delta^{-1} \begin{vmatrix} \gamma_{33} & \gamma_{34} \\ \gamma_{34} & \gamma_{44} \end{vmatrix} \begin{vmatrix} F_3 \\ F_4 \end{vmatrix} + \begin{vmatrix} \beta_{13} & \beta_{14} \\ \beta_{23} & \beta_{24} \end{vmatrix} \Delta^{-1} \begin{vmatrix} \gamma_{3r} & \gamma_{3s} \\ \gamma_{4r} & \gamma_{4s} \end{vmatrix} \begin{vmatrix} F_r \\ F_s \end{vmatrix} \tag{2.37}$$

In order to find $\begin{bmatrix} \alpha_{11} & \alpha_{12} \\ \alpha_{12} & \alpha_{22} \end{bmatrix}$, $\begin{vmatrix} F_3 \\ F_4 \end{vmatrix}$ is set to equal zero and $\begin{vmatrix} F_r \\ F_s \end{vmatrix}$ is set to equal zero as well so:

$$\begin{vmatrix} U_1 \\ U_2 \end{vmatrix} \begin{vmatrix} \frac{1}{F_1} & \frac{1}{F_2} \end{vmatrix} = \begin{vmatrix} \beta_{11} & \beta_{12} \\ \beta_{12} & \beta_{22} \end{vmatrix} \begin{vmatrix} F_1 \\ F_2 \end{vmatrix} \begin{vmatrix} \frac{1}{F_1} & \frac{1}{F_2} \end{vmatrix} - \begin{vmatrix} \beta_{13} & \beta_{14} \\ \beta_{23} & \beta_{24} \end{vmatrix} \Delta^{-1} \begin{vmatrix} \beta_{13} & \beta_{23} \\ \beta_{14} & \beta_{24} \end{vmatrix} \begin{vmatrix} F_1 \\ F_2 \end{vmatrix} \begin{vmatrix} \frac{1}{F_1} & \frac{1}{F_2} \end{vmatrix} \tag{2.38}$$

Finally,

$$\begin{vmatrix} \frac{U_1}{F_1} & \frac{U_1}{F_2} \\ \frac{U_2}{F_1} & \frac{U_2}{F_2} \end{vmatrix} = \begin{vmatrix} \alpha_{11} & \alpha_{12} \\ \alpha_{12} & \alpha_{22} \end{vmatrix} = \begin{vmatrix} \beta_{11} & \beta_{12} \\ \beta_{12} & \beta_{22} \end{vmatrix} - \begin{vmatrix} \beta_{13} & \beta_{14} \\ \beta_{23} & \beta_{24} \end{vmatrix} \Delta^{-1} \begin{vmatrix} \beta_{13} & \beta_{23} \\ \beta_{14} & \beta_{24} \end{vmatrix} \tag{2.39}$$

The same steps are repeated for calculating $\begin{bmatrix} \alpha_{13} & \alpha_{14} \\ \alpha_{23} & \alpha_{24} \end{bmatrix}$ and by setting, $\begin{vmatrix} F_1 \\ F_2 \end{vmatrix}$ and $\begin{vmatrix} F_r \\ F_s \end{vmatrix}$ equal to zero.

$$\begin{vmatrix} U_1 \\ U_2 \end{vmatrix} = \begin{vmatrix} \beta_{13} & \beta_{14} \\ \beta_{23} & \beta_{24} \end{vmatrix} \Delta^{-1} \begin{vmatrix} \gamma_{33} & \gamma_{34} \\ \gamma_{44} & \gamma_{44} \end{vmatrix} \begin{vmatrix} F_r \\ F_s \end{vmatrix} \tag{2.40}$$

The same steps are repeated for calculating $\begin{bmatrix} \alpha_{1r} & \alpha_{1s} \\ \alpha_{2r} & \alpha_{2s} \end{bmatrix}$ by setting, $\begin{vmatrix} F_1 \\ F_2 \end{vmatrix}$ and $\begin{vmatrix} F_3 \\ F_4 \end{vmatrix}$ equal to zero.

$$\begin{vmatrix} U_1 \\ U_2 \end{vmatrix} = \begin{vmatrix} \beta_{13} & \beta_{14} \\ \beta_{23} & \beta_{24} \end{vmatrix} \Delta^{-1} \begin{vmatrix} \gamma_{3r} & \gamma_{3s} \\ \gamma_{4r} & \gamma_{4s} \end{vmatrix} \begin{vmatrix} F_r \\ F_s \end{vmatrix} \tag{2.41}$$

Substituting Equation (2.36) in Equation (2.31) leads to

$$\begin{vmatrix} \alpha_{pr} & \alpha_{ps} \\ \alpha_{qr} & \alpha_{qs} \end{vmatrix} = \begin{vmatrix} \gamma_{pr} & \gamma_{ps} \\ \gamma_{qr} & \gamma_{qs} \end{vmatrix} - \begin{vmatrix} \gamma_{3p} & \gamma_{4p} \\ \gamma_{3q} & \gamma_{4q} \end{vmatrix} \Delta^{-1} \begin{vmatrix} \gamma_{3r} & \gamma_{3s} \\ \gamma_{4r} & \gamma_{4s} \end{vmatrix} \tag{2.42}$$

Since all the reacceptances required are present, the solution can be done using matrix methods [3]

4.2.4 Results

A code utilizing systems receptance coupling approach for analyzing the spindle system presented in Figure 19. is written to obtain the response of the system over a frequency range of 800 Hz as illustrated in Figure 22, the values of the first resonant frequency can be extracted.

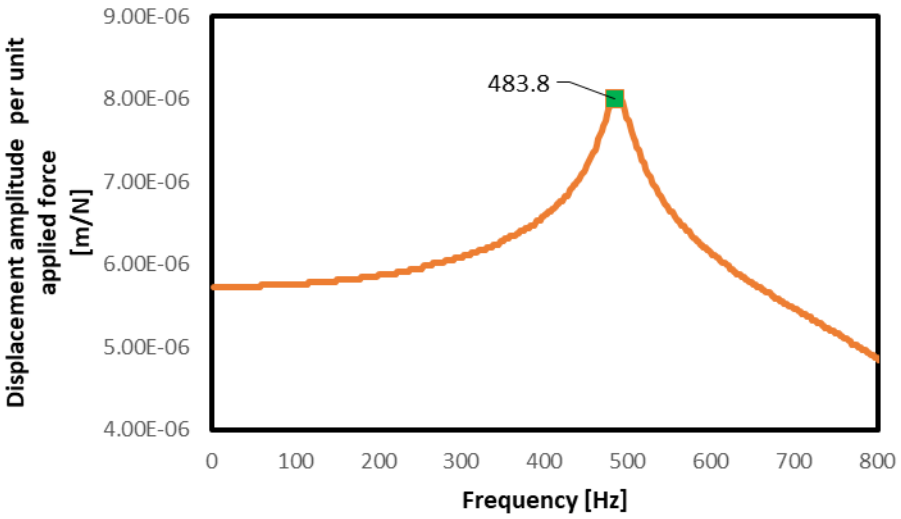

Figure 22. Displacement amplitude per applied force response of the proposed spindle system.

Finite element modal analysis of the proposed model is performed using ANSYS V19 software to compare the result of the first natural frequency value. The following settings are set for the analysis:

- The geometry in Figure 19 is used.

- Structural steel material is used with a density of 7.85e-06 kg/mm³, Young's Modulus of 2e+05 MPa, tensile yield strength of 250 MPa and a tensile ultimate strength of 460 MPa.
- For the connections, three bearings connections are used with the same exact locations listed in Figure 19. The connection type is Body-Ground and the value of the stiffness is set to 7.5e+008N/m.
- Mesh details: The mesh is generated using ANSYS V19, the elements are tetrahedral with a total element count of 28712 and a node count of 59336. The element size is 10 mm while the average surface area of the model is 7500.5 mm². Mesh quality was assessed using skewness. The skewness metric showed a minimum value of 4.0296e-004, a maximum of 0.99501, an average of 0.30625, and a standard deviation of 0.18708. Figure 23 shows the meshed spindle model.

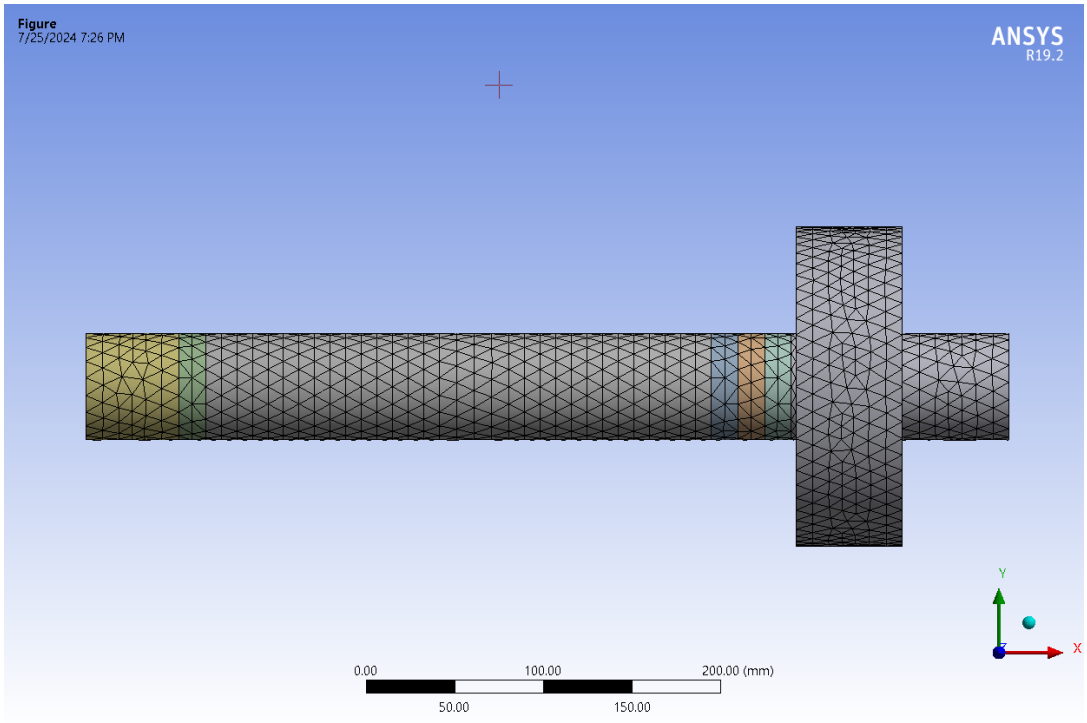

Figure 23. The meshed spindle system.

Figure 24. shows the first resonant frequency mode shape obtained from ANSYS 19.

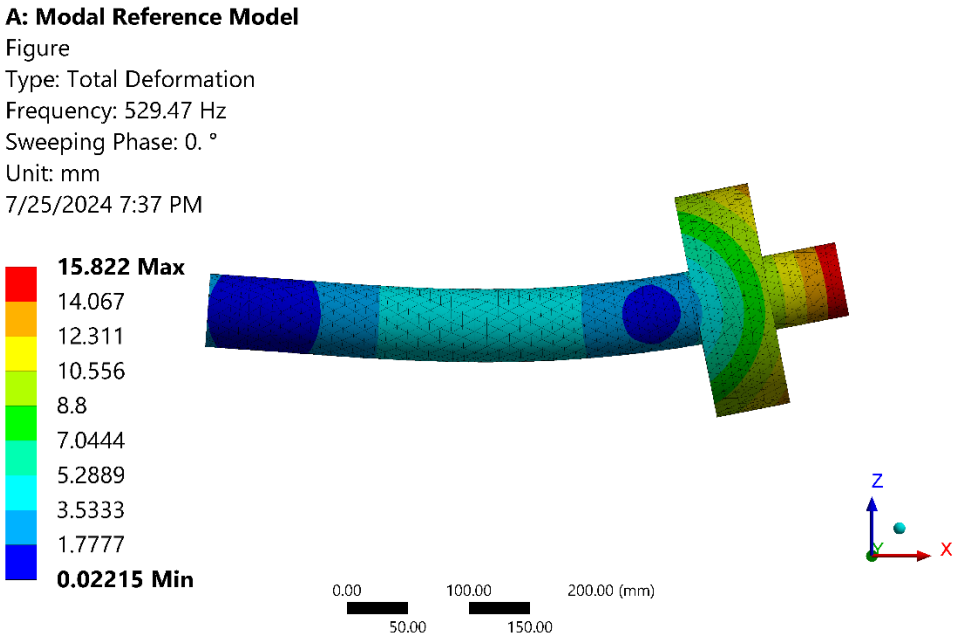

Figure 24. ANSYS 19 spindle system mode shape.

Table 6 compares the results of first resonant frequency [Hz] of the spindle system using the systems receptance; coupling approach and the results from the finite element analysis using ANSYS software.

Table 6. Results comparison.

Mode number	Receptance approach	ANSYS	Error %
1	483.3	529.47	8.7%

4.2.5 Conclusion

A spindle system supported on three bearings is analyzed using the systems receptance coupling approach. This analysis considers the stiffness of the bearings and aims to determine the first resonant frequency. The same spindle system is also analyzed using the finite element method (FEM) with ANSYS software. The results of the two approaches are then compared. The comparison of the results shows a good agreement in the values of the resonant frequencies. Specifically, the first resonant frequency obtained from the receptance approach is 483.3 Hz, while the ANSYS FEM analysis yields a frequency of 529.47 Hz. This results in an error percentage of 8.7%, indicating a reasonably close match between the two methods.

The code used to analyze the spindle system suing the systems receptance coupling approach can be modified to take into account for different bearing stiffness (different kinds of bearings) values and location and different lengths and diameters of shaft segments, chuck and workpiece

which can be helpful in the process of optimizing the spindle system in terms of resonant frequencies values. The code is written in *JAVA* with an algorithm that starts with initializing the parameters by setting initial values for frequency, lengths of the shaft segments, bearings locations and stiffness values of the bearings. Then, data is collected and processed by storing response data and natural frequency values.

4.2.6 Related Publications

Alzghoul, Mohammad and Sarka, Ferenc and Szabó, Ferenc János (2022) A Spindle System Analysis Using Systems Receptance Coupling Approach. DESIGN OF MACHINES AND STRUCTURES: A PUBLICATION OF THE UNIVERSITY OF MISKOLC, 12 (2). pp. 25-32. ISSN 1785-6892 (print); 2064-7522 (online)

5 OPTIMIZATION AND RESULTS

5.1 Introduction

The objective of this chapter is to enhance the performance of a lathe spindle system by addressing two key aspects: minimizing chatter occurrence (when the excitation frequency aligns with the natural frequency of the spindle) and improving stress capacity. These improvements will be pursued while maintaining the same overall mass of the system. The optimization of the spindle system design will be carried out through two distinct methods:

1. Utilizing the Kuhn-Tucker optimality criterion in conjunction with the Grapho-Analytical technique.
2. Employing the RSM (Response Surface Methodology) and ANOVA (Analysis of Variance) technique as they are complementary methods used in statistical analysis and experimental design.

By employing these two approaches, the aim is to identify and implement structural modifications that can effectively optimize the lathe spindle system.

5.2 The Proposed Spindle System Design and Analysis

The proposed model of the lathe spindle consists of a shaft of uniform thickness, three bearings, a chuck, and a workpiece. Figure 25 shows a section view of the model. It illustrates the arrangement and dimensions of the components that form the lathe spindle model.

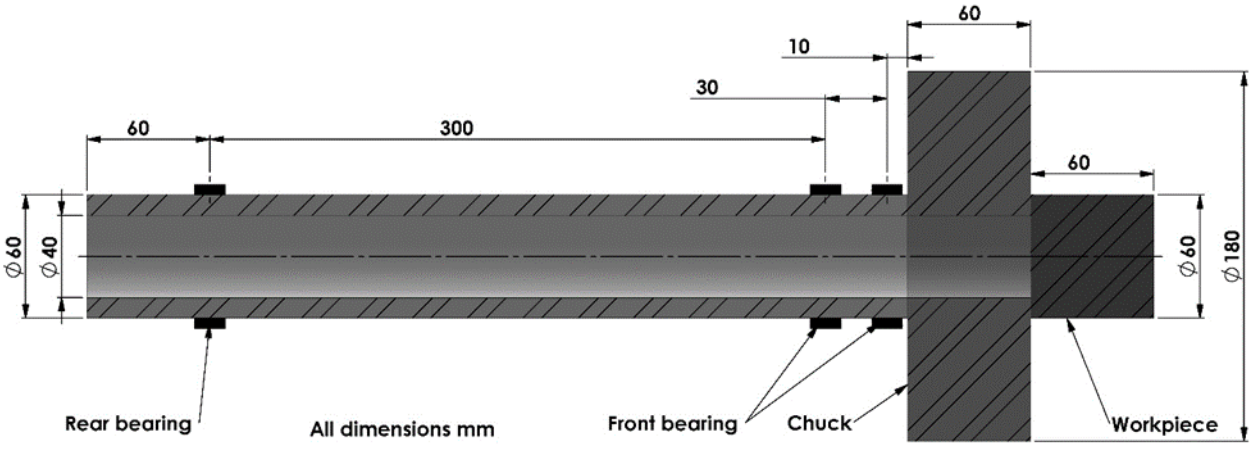

Figure 25. Section View of Lathe Spindle Proposed Model.

The main reason for selecting this model is that it is used in the literature in [3] and in [95]. Therefore, it can serve as a good reference model.

Some limits for the optimization are taken into considerations to ensure proper functioning of the shaft in the proposed spindle model. First, the minimum inner diameter of the shaft should not be less than 40 mm, as this is necessary for the bar feeding mechanism. Additionally, the shaft thickness must not be less than 7 mm, considering the maximum allowable angle of twist is 0.25 degree/meter [98]. The torque applied to the spindle is 576 Nm (Based on the data sheet of Haas ST-35L CNC lathe [99]). Finally, the assumed bearing stiffness is 7.5+008 N/m [3].

Calculating natural frequency values is crucial as a first step to shift them away from expected excitations during machining.

Equation (5.1) represents the vibration differential equation for the spindle system. This can be used to determine the natural frequency values.

$$[\boldsymbol{M}]\{\ddot{\boldsymbol{X}}\} + [\boldsymbol{R}]\{\dot{\boldsymbol{X}}\} + [\boldsymbol{K}]\{\boldsymbol{X}\} = \{\boldsymbol{F}\} \quad \textbf{(5.1)}$$

In rotor dynamics, equation (5.1) can be expressed in the following form:

$$[\boldsymbol{M}]\{\ddot{\boldsymbol{X}}\} + \left([\boldsymbol{R}] + \left[\boldsymbol{R}_{\boldsymbol{gyro}}\right]\right)\{\dot{\boldsymbol{X}}\} + ([\boldsymbol{K}] + [\boldsymbol{H}])\{\boldsymbol{X}\} = \{\boldsymbol{F}\} \quad \textbf{(5.2)}$$

Equations (5.1) and (5.2) serve as the foundation for calculating the natural frequency of spindle systems; additionally, they account for the gyroscopic effect. The gyroscopic effect, a phenomenon resulting from the conservation of angular momentum, occurs when a rotating object resists changes to its axis of rotation. This effect leads to precession, where the axis of rotation shifts perpendicular to the applied force rather than tilting directly in its direction. In spindle systems, the gyroscopic effect significantly influences stability, vibration, and natural frequencies by altering the effective stiffness and damping properties, which must be considered to avoid resonant conditions and potential mechanical failure. This effect is critical in applications requiring high precision and control, such as high-speed machining [100].

5.3 The Grapho- Analytical Optimization Method

Graphical representations of optimization problems can aid in the search for better solutions during the design of critical machine elements. By visually mapping out the problem, a deeper understanding can be gained of the variables and constraints. Graphical representations can quickly identify the most promising solutions, resulting in more efficient and effective machine elements.

A useful way to represent constrained optimization problems is to draw a single diagram that includes both the isolines of the objective function and the borders of the feasible region. This approach provides a simple yet powerful definition of the optimality criterion for straightforward optimization tasks. By using this method, insights can be quickly gained into the trade-offs between competing constraints and optimize the design.

The theoretical foundation of the grapho-analytical method suggests that the Kuhn-Tucker optimality criterion is pivotal. This criterion suggests that at the optimal point, the iso-line of the objective function tangentially intersects the feasible region. This tangency may show as a shared point between the iso-line and a border of the region, or as the iso-line touching the region at one of its corner points. Understanding this criterion is crucial as it explains the conditions under which optimal solutions are attained within the framework of grapho-analysis.

This approach, hybridizing graphical and analytical ways, delves into the fundamental aspects of constrained optimization, focusing on the concept of iso-lines for the objective function and the boundaries of constraints. It identifies a specific point along the iso-line and at the edge of the feasible region, where the objective function achieves its maximum or minimum value. This point represents the optimum value of the objective function within the constraints. The method is divided into two main strategies: the graphical approach, which employs diagrams to illustrate the iso-lines of the constraints and the objective function, allowing for an intuitive understanding of the optimum's location, and the analytical approach, which involves algebraic manipulation and simplification of the equations pertaining to the constraints and objective function to pinpoint the exact optimum. The grapho-analytical method combines these two approaches to provide both a clear visual representation and precise mathematical determination of the best solution, thereby simplifying optimization problems. This dual approach is particularly beneficial for educational purposes or as a foundational step in tackling more complex problems.

To employ this method, the objective function and its contours must be defined, along with the optimization constraints.

5.3.1 The Optimization of the Proposed Model (First Natural Frequency Value) (Graphically)

Establishing the optimization system involves two primary steps. First, setting the constraints of the optimization problem. Second, defining the objective function and its contours.

5.3.1.1 The first set of parameters

For the proposed model, the goal is to increase the inner diameter of the shaft near the chuck while reducing its thickness to maintain the overall shaft mass. The idea behind the proposed model in terms of rigidity and strength is the following:

- Uniform Shaft: A uniform shaft maintains the same diameter and shape across its length, ensuring consistent cross-sectional area and moment of inertia. This uniformity is crucial for its rigidity, allowing it to resist bending and torsion effectively, especially when the load it bears is constant or evenly distributed.
- Tapered Shaft: the design of the tapered shaft, featuring an increasing diameter towards the chuck with a compensating thinner wall, results in varying cross-sectional area and moment of inertia along its length. Near the chuck, where the diameter is larger, the shaft demonstrates enhanced rigidity due to the increased moment of inertia, offering superior resistance to bending and torsion in the crucial area facing the highest machining forces.

Overall, the tapered shape is selected because it maintains the initial diameter of the uniform shaft, which is essential for the bar feeding mechanism to function properly. Additionally, its geometrical properties provide superior rigidity and bending resistance compared to the uniform shaft. These differences are discussed in the subsequent sections.

Two variables are introduced that relate to each other through by the pre-optimized shaft system volume is 628318.53 mm^3. The variables are the bigger radius of the cone, denoted R, and the cone thickness, denoted t. Figure 26 illustrates the truncated hollow cone under consideration.

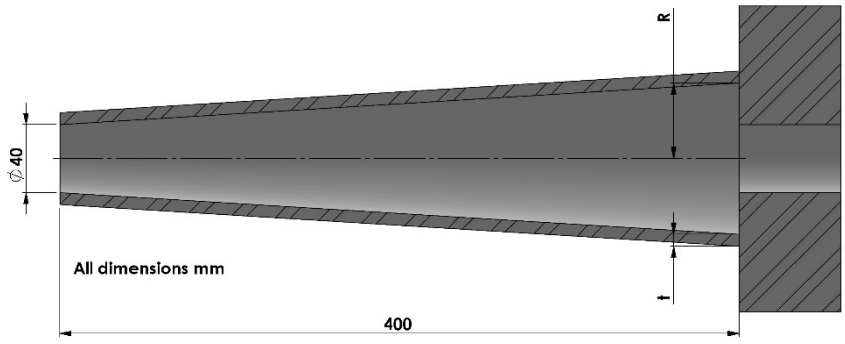

Figure 26. Section view of the truncated Hollow Cone Representation for Optimizing Spindle Shaft Design.

The relationship between the variables is derived from the volume equation and is presented in Equation (5.3).

$$\boldsymbol{Volume} = \left(\frac{\pi L}{3}\left((\boldsymbol{R}+\boldsymbol{t})^2 + (\boldsymbol{27.5}+\boldsymbol{t})^2 + (\boldsymbol{R}+\boldsymbol{t}) + (\boldsymbol{27.5}+\boldsymbol{t})\right)\right) - (\frac{\pi L}{3}(\boldsymbol{R^2} + \boldsymbol{27.5^2} +$$

$$\boldsymbol{27.5R} \xrightarrow{\boldsymbol{yields}} \quad \boldsymbol{R} = -\frac{(\boldsymbol{t}+\boldsymbol{34.5})(\boldsymbol{t}-\boldsymbol{14.5})}{\boldsymbol{t}} \tag{5.3}$$

Additional constraints are introduced as follows:

$$\boldsymbol{R} \geq \boldsymbol{20\ mm} \tag{5.4}$$

$$\boldsymbol{7\ mm} \leq \boldsymbol{t} \leq \boldsymbol{10\ mm} \tag{5.5}$$

To establish the objective function, the spindle system is analyzed using the Finite Element Method using ANSYS V19 software for various R and t values to determine the first natural frequency. Table 7 lists the values of t and frequency used to establish the objective function by fitting t and frequency values in a second-degree polynomial which is Equation (5.6). The process involves polynomial regression, a form of linear regression used to model a non-linear relationship between the independent variable R and the dependent variable t.

Table 7. t and frequency values used to establish the objective function equation.

t [mm]	R [mm]	Frequency [Hz]
7.00	44.46	324.52
7.25	41.750	323.3
7.50	39.20	321.91
7.75	36.79	320.43
8.00	34.53	318.8

$$\boldsymbol{R(t)} = \boldsymbol{-1.04t^2 - 9.876t + 306.35} \tag{5.6}$$

The optimization process is visualized in Figure 27, which shows a plot of the objective function and its contours alongside the implicit and explicit constraints. The plot provides a graphical representation of the optimization problem, allowing for a better understanding of the relationship between the objective function and the constraints.

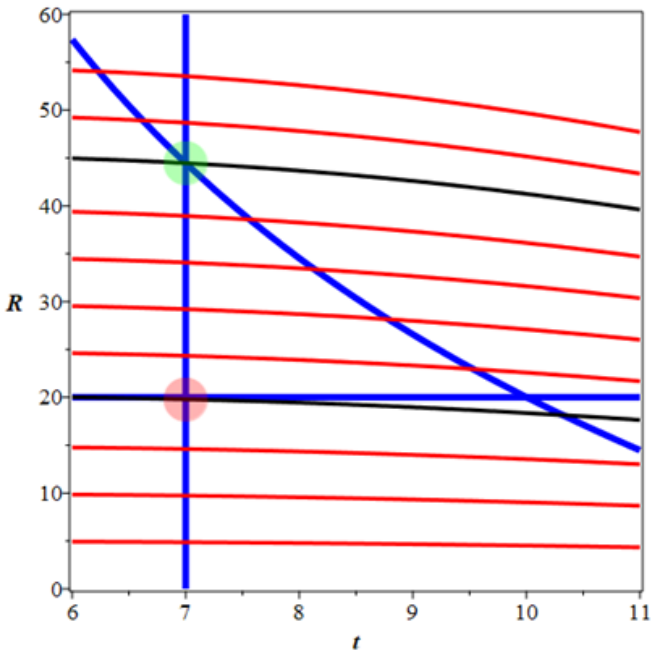

Figure 27. The plot of the thickness and diameter next to the chuck constraints and the objective function contours of the first natural frequency.

In Figure 27, the feasible solution region is represented by the enclosed area between the blue lines and curve, denoting the constraint borders. The red curves depict objective function contours. The black curves represent optimal objective function contours. The green circle indicates the optimal point (maximum point), which is the intersection of two constraints and one objective function contour. At the green circle, t and R values are 7 mm and 44.46 mm, respectively. This implies the highest first natural frequency value occurs when shaft thickness is 7 mm and the radius near the chuck is 44.46 mm. The red point is an optimal point represents the minimum.

5.3.1.2 The second parameter, the rear bearing location

The second parameter is to investigate the location of the rear bearings, the main steps of the previous section are repeated in order to construct the objective function. For the constraints, the first constraint is the axial location of the bearing taking the left end of the shaft as a reference, then the constraint of the axial location of the bearing is expressed as:

$$\mathbf{7.5}\ \boldsymbol{mm} \leq \boldsymbol{L} \leq \mathbf{200}\ \boldsymbol{mm} \tag{5.7}$$

The axial location range starts at 7.5 mm, as this is the bearing center, and ends at 200 mm, the shaft midpoint. When the rear bearing is fitted much beyond the midpoint of the shaft, it is more liable to deflection since there is greater leverage provided by forces put on the tool. By

locating the rear bearing at or before the midpoint, it helps in the distribution of the support to reduce, especially when the lathe is under heavy cutting force.

Another constraint is the relationship between the axial location and the radius of the shaft associated with each axial location. (The shaft has a conical shape at this point as a result of optimizing the first parameter.) This relationship is expressed as (Derived in appendix A):

$$\boldsymbol{D = 0.0612L + 20} \tag{5.8}$$

To establish the objective function, the spindle system is analyzed using the Finite Element Method using *ANSYS V19* software for a range of R and L values to determine the first natural frequency. Table 8 lists the values of L and frequency used to establish the objective function by fitting D and frequency values in a third-degree polynomial which is Equation (5.9). That was archived by polynomial regression, a form of linear regression used to model a non-linear relationship between the independent variable L and the dependent variable D.

Table 8. L and frequency values used to establish the objective function equation.

L[mm]	D[mm]	Frequency [Hz]
7.5	20.46	712.16
50	23.06	767.71
100	26.12	819.04
150	29.18	850.01
200	32.24	826.90

$$\boldsymbol{D(L) = \left(-0.3 * 10^{-5}\right)L^3 - 0.0027L^2 - 1.1843L + 703.62} \tag{5.9}$$

The optimization process is visualized in Figure 28, which shows a plot of the objective function and its contours alongside the implicit and explicit constraints. The plot provides a graphical representation of the optimization problem, allowing for a better understanding of the relationship between the objective function and the constraints.

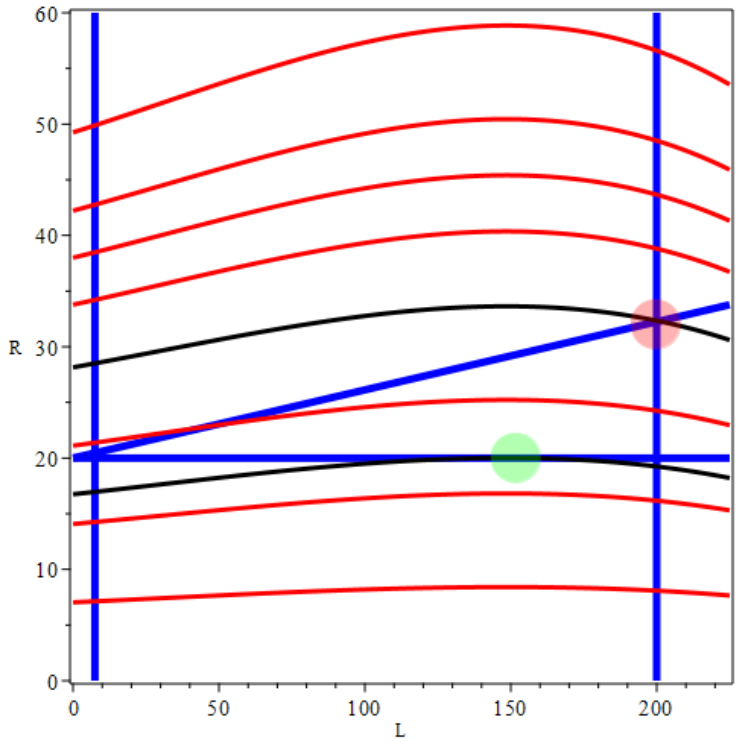

Figure 28. The plot of the rear bearing location constraints and the objective function contours of the first natural frequency.

In Figure 28, the feasible solution region is represented by the enclosed area between the blue lines denoting constraint borders. The red curves depict objective function contours. The black curves represent optimal objective function contours. The green circle indicates the optimal point (maximum point), as it is tangent to the feasible region. This implies that when the two curves are equal, there is only one solution where they intersect. At the green circle, L value is 162 mm. This implies the highest first natural frequency occurs when the rear bearing center is located 162 mm from the shaft left end. The red point is an optimal point representing the minimum.

5.3.2 The Optimization of the Proposed Model (Analytically)

The confirmation of the results of the graphical solution should be ensured by the analytical solution. To optimize the spindle system for the value of the first natural frequency through analytical means, an implicit constraint Equation (5.3) should be set equal to the objective function Equation (5.6) after being multiplied by a factor "C" responsible for shaping the contours of the objective function. Equation (5.10) represents the outcome of this process.

$$-\frac{(t+34.5)(t-14.5)}{t} = (-1.04t^2 - 9.876t + 306.35) * C \qquad \textbf{(5.10)}$$

In the analytical solution, the primary objective is to obtain a single solution of Equation (5.10) for the variable "t" within the domain of 7 to 10 mm that at the same time intersects with the constraint vertical line at x =7. To achieve this goal, an algorithm has been devised and depicted in Figure 29, which aids in determining the optimal solution.

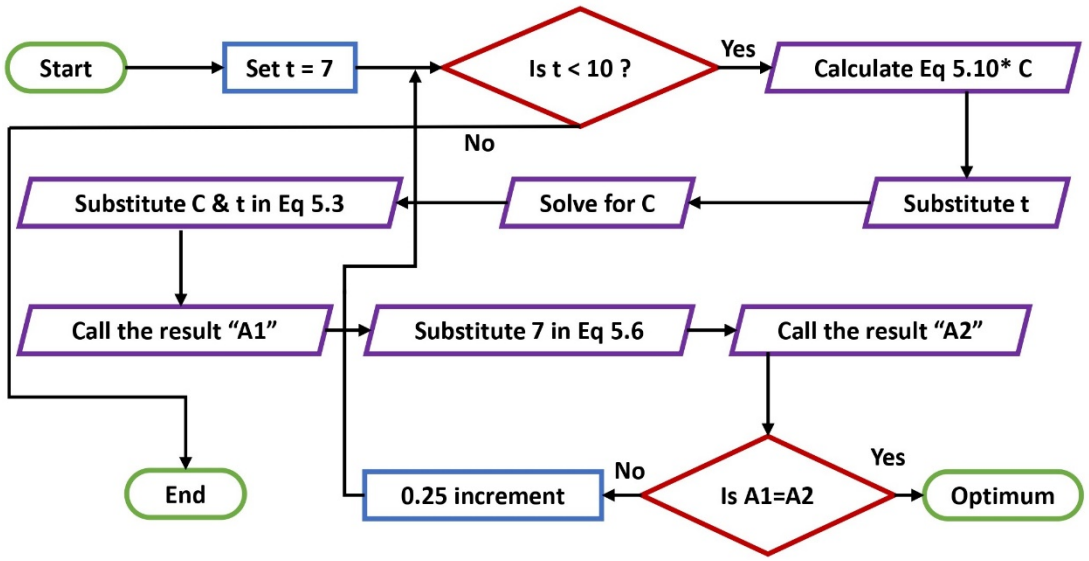

Figure 29. The optimum solution finding algorithm.

After performing the solution, the value of C is 0.137 and the corresponding t value is 7 mm. Based on Equation (5.3) the value of R is 44.46 mm which matches the result of the graphical method.

The same procedure is applied for the second parameter (the rear bearing location). The optimum rear bearing location is 7.5 mm from the left end of the shaft.

5.4 RSM and ANOVA Optimization

This part of the research utilizes response surface methodology (RSM) in conjunction with analysis of variance (ANOVA) to optimize the design of the proposed lathe spindle system. For RSM, it is a collection of mathematical and statistical techniques useful for developing and optimizing processes. It helps in modeling and analyzing problems in which a response of interest is influenced by several variables. The main idea is to use a sequence of designed experiments to obtain an optimal response. It works as follows:

- Design of Experiments (DOE): The process begins with designing an experiment to systematically vary the input variables.

- Fitting a Model: The data obtained from the experiments are used to fit a model) that approximates the response surface.
- Analyzing the Response Surface: The model helps in understanding the effect of input variables and their interactions on the response. The goal is to find the optimal conditions for the desired response.
- Optimization: Using the model, the optimal levels of the input variables are determined to achieve the best possible response.

For ANOVA, it is a statistical technique used to determine the significant factors affecting the response variable. It works as follows:

- Partitioning Variability: ANOVA divides the total variability in the data into components attributable to different sources.
- Hypothesis Testing: It tests the null hypothesis that all group means are equal against the alternative hypothesis that at least one group mean is different.
- F-statistic: ANOVA calculates an F-statistic to determine the significance of the factors. A higher F-value indicates a more significant factor.

RSM and ANOVA are often used together since RSM: Provides a model and optimization pathway by systematically varying input variables and analyzing their effects. Also, ANOVA identifies which variables and interactions are statistically significant, refining the RSM model and focusing the optimization efforts [101].

RSM is employed to develop an empirical model that characterizes the relationship between key parameters (shaft geometry and bearing location) and the natural frequency response of the system. This modeling is accomplished through statistically designed experiments and regression analysis [102]. ANOVA enables the determination of the statistical significance of individual parameters and their interactions on the frequency response [103]. Taken together, RSM allows the complex relationships between inputs and response to be modeled, while ANOVA highlights the most critical factors [104]. This approach enables the systematic optimization of parameters to maximize natural frequency and chatter reduction within operational constraints.

5.4.1 The Optimization of the Proposed Model (First Natural Frequency Value)

Design expert software is employed to run the analysis and generate response surfaces. The design variables remain unchanged: shaft thickness, shaft diameter next to the chuck, and rear bearing location. To preserve constant mass when varying thickness and diameter near the chuck, optimization is done in two stages. The first stage optimizes rear bearing location. The second stage optimizes shaft thickness and diameter next to the chuck.

5.4.1.1 Stage Number One, Optimizing the Rear Bearing Location

In order to construct the response surface, a mathematical model that approximates the relationship between the input factors (independent variables) and the response variable (dependent variable) is to be developed. In this study, a quadratic mathematical model is selected due to its ability to capture curved relationships between variables. Then the model is validated by the analysis of variance (ANOVA), this ensures that the coefficients are statistically significant. The following steps are carried out to perform the analysis and to construct the response surface.

1. Defining objectives and factors:
   The objective of the optimization is to maximize the first natural frequency of the lathe spindle system. The factors taken into consideration are radius next to the chuck and the location if the rear bearing.
2. The design of the experimental layout:
   The selected design type is central composite due to its efficiency in factorial analysis, flexibility in factorial arrangement and optimization capability. Figure 30 illustrates the structure of central composite design.

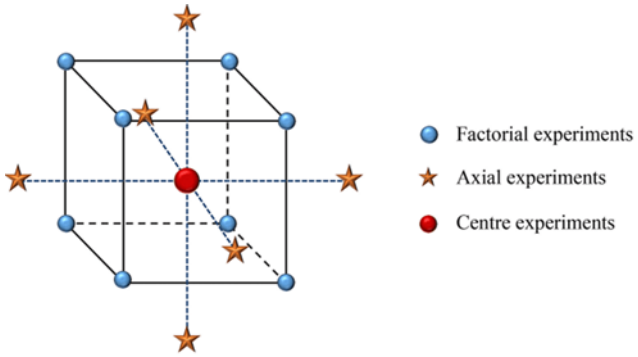

Figure 30. Structure of central composite design [105].

The first component of central composite design is the so-called, factorial experiments (points), these points are located at the vertices of the design space. They help in estimating the interaction effect of the factor of the experiment. The second component is the so-called, axial experiment (Star points), these points are located along the axes of the design space, their main objective is to allow for the estimation of the curvature of the response surface. The third component is the so-called, center experiments (center points), which are included to provide an estimate of the experimental error and the pure error of the response surface [105]. For the ranges of the factors selected, they are the same ranges as mentioned in the Grapho – analytical technique as the main goal is to compare the results of the RSM and the Grapho – analytical technique.

3. Conducting the experiment:

   The experiments of Table 9 are conducted using *ANSYS V19* software in order to establish the required data to run the *ANOVA* analysis and to generate the response surface. The proposed spindle model was modified in terms of its radius next to the chuck and its rear bearing location according to the data provided in Table 9, specifically the data in columns two and three. Due to the Central Composite Design model, and since the axial points are placed outside the experiment space, some runs in Table 9 are outside the limits of the optimization constraints.

Table 9. Runs used to construct the response surface 1

RUN	Factor 1 A: Radius [mm]	Factor 2 B: Rear bearing location [mm]	Response 1 Frequency [Hz]
1	32.2	32.3	642.7
2	20	7.5	506.2
3	32.2	103.7	706.1
4	44.4	7.5	712.1
5	20	200	612.0
6	14.9	103.7	488.9
7	32.2	239.8	654.4
8	44.4	200	826.9
9	49.5	103.7	860.9

Figure 31 illustrates the response surface for optimizing rear bearing location. Axis A represents the shaft radius associated with the rear bearing location. Axis B represents the rear bearing location. The third, vertical axis represents frequency.

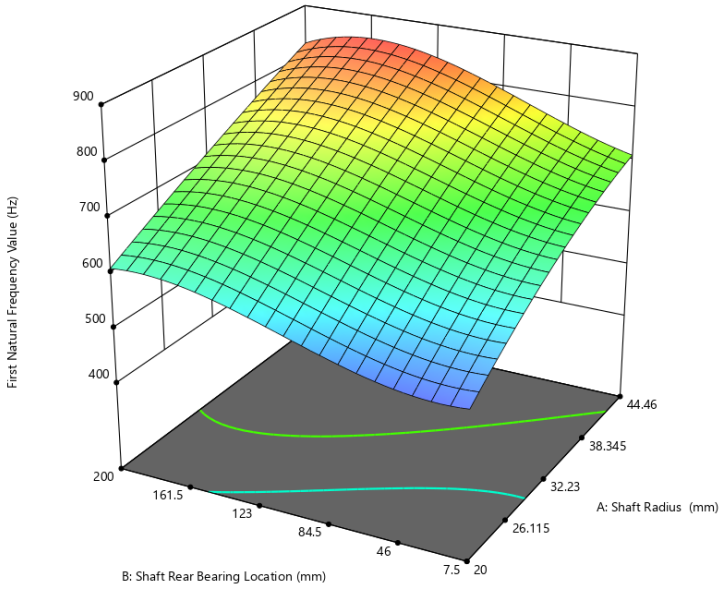

Figure 31. The response surface of optimizing the rear bearing location.

As observed in Figure 31, the surface height peaks (red zone) when the shaft radius next to the chuck is 44.46 mm and the rear bearing location ranges from 155-165 mm from the shaft end.

5.4.1.2 Stage Number Two, Optimizing the Geometry of The Shaft

The same steps of section 5.4.1.1 are repeated in this section taking into consideration the different runs for constructing the response surface as listed in Table 10.

Table 10. Runes used to construct the response surface 2

RUN	Factor 1 A: Thickness of the shaft [mm]	Factor 2 B: Radius [mm]	Response 1 Frequency [Hz]
1	8.5	32.23	676.821
2	10	20	535.424
3	7	20	448.772
4	8.5	49.5258	692.912
5	7	44.46	760
6	8.5	14.9342	406.017
7	6.37868	32.23	760
8	10.6213	32.23	747.674
9	10	44.46	586.935

Figure 32 illustrates the response surface for optimizing shaft geometry. Axis A represents shaft thickness. Axis B represents the shaft radius next to the chuck. The third, vertical axis represents frequency.

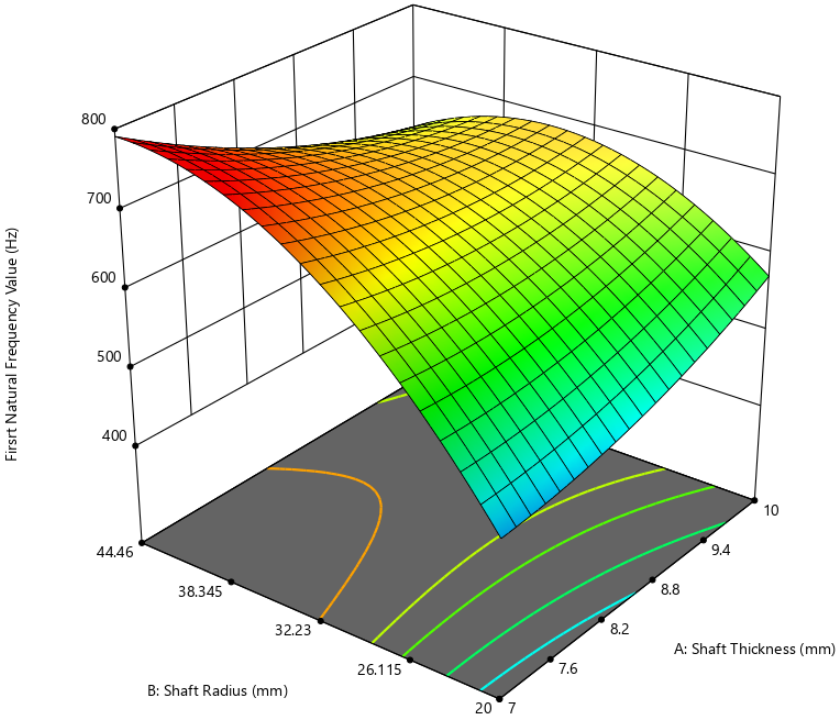

Figure 32. The response surface of optimizing the geometry of the shaft.

As observed in Figure 32, the response surface height peaks when the shaft radius next to the chuck is 44.46 mm and shaft thickness is 7 mm.

5.4.1.3 Comparison of the Results of the Two Optimization methods

In this subsection, a comparison of the results of the two optimization methods is carried out. Table 11 lists the optimization methods and their results.

Table 11. Comparison of Optimization Methods and Their Corresponding Natural Frequencies.

Parameter / Method	Optimized R [mm]	Optimized t [mm]	Optimized L [mm]	1st Natural Frequency [Hz]
The Grapho- Analytical Method	44.46	7	162	-
RSM and ANOVA Method	44.46	7	161	792

In comparing the two optimization methods, the Grapho-Analytical Method and the Response Surface Methodology (RSM) with Analysis of Variance (ANOVA), distinct strengths and limitations emerge. The Grapho-Analytical Method provides optimized parameters—namely, a radius of the shaft next to the chuck of 44.46 mm, a thickness of the shaft of 7 mm, and a rear bearing location of 162 mm—aimed at achieving an optimal first natural frequency. However,

it does not directly yield the value of this frequency. Instead, these parameters are intended for use with further methods, such as Finite Element Analysis (FEA), to determine the actual first natural frequency. On the other hand, the RSM and ANOVA Method not only delivers optimized parameters but also estimates the first natural frequency to be 792 Hz. This estimate provides a useful indication but is not the final value. For precise frequency determination, FEA is necessary, which, in this case, reveals the actual first natural frequency to be 852.52 Hz as indicated in the next subsection. This result suggests that while the RSM and ANOVA Method offers a close approximation, FEA is essential for accurate validation and refinement of the natural frequency predictions.

5.5 Results Evaluation

In this section, the optimization results are evaluated and compared to the non-optimized model, providing better insight into how optimization enhanced performance of the proposed model regarding stress capacity and chatter occurrence. Figure 33 illustrates the non-optimized and optimized models, including geometrical dimensions.

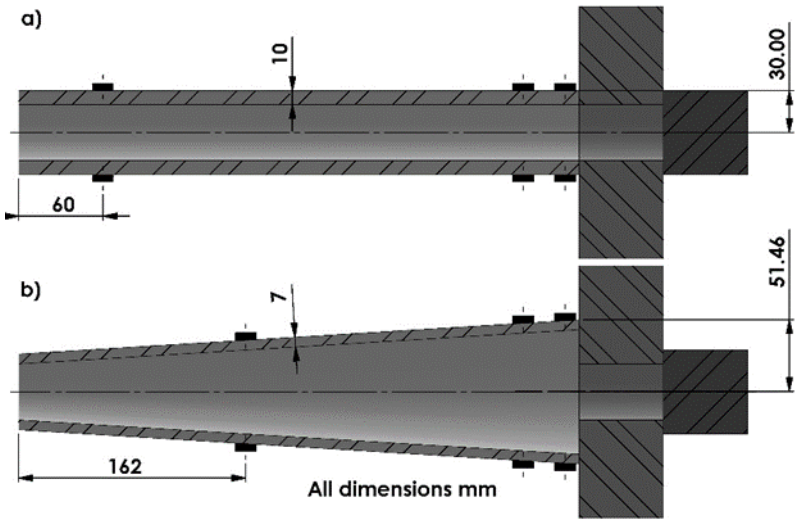

Figure 33. a) The non-optimized model, b) The optimized model.

As shown in Figure 34, the first natural frequency of the optimized model is 323.05 Hz higher than the non-optimized model, representing a 60.5% increase.

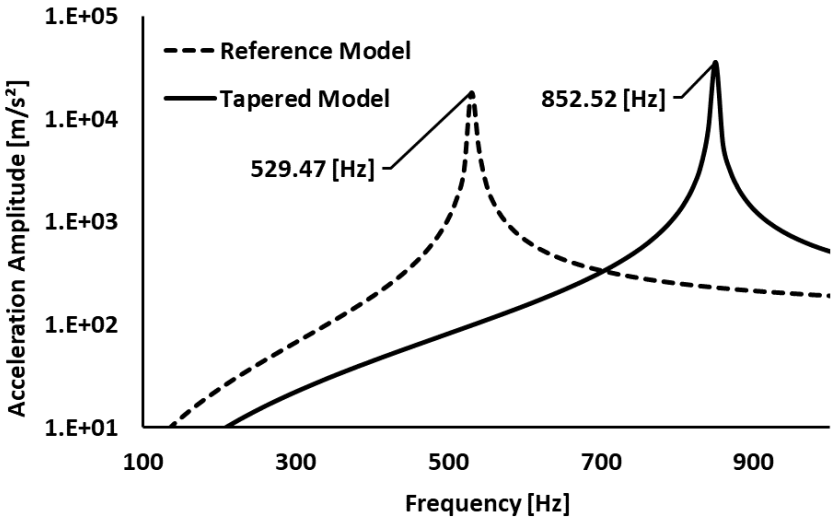

Figure 34. Frequency response of the optimized and the non-optimized models.

A 15.375 kN load is applied to the non-optimized model workpiece to better understand the optimized enhanced stress capacity of the model. This load was chosen because it causes permanent spindle system deformation (the yield point). The optimized model is then subjected to the same load. Because the purpose is to compare both spindle models, the supports are assumed to be rigid in both cases. Figure 35 illustrates the boundary conditions as well as the results of applying this load to optimized and non-optimized models.

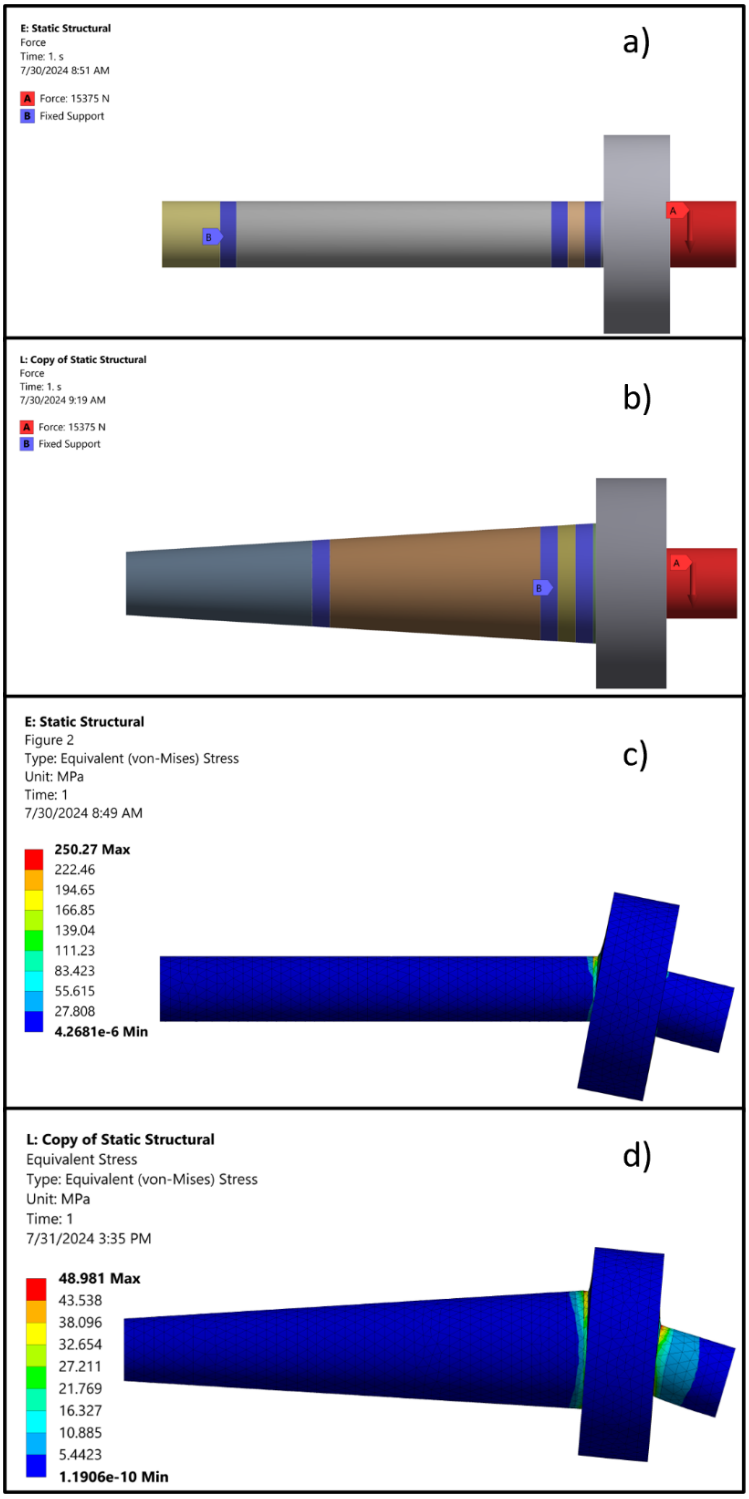

Figure 35. a) the reference spindle model boundary conditions, b) the proposed spindle model boundary conditions, c) the deformation stress analysis result, the reference model, d) the deformation stress analysis result, the proposed spindle model.

As observed in Figure 35, a relatively large enhancement in stress capacity is achieved after optimization. In summary, Table 12 compares the optimized and non-optimized models.

Table 12. Model Performance Comparison: Optimized and Non-Optimized Models.

Property Model	Stress [MPa]	1st Natural frequency [Hz]
Non-optimized	250	529.47
Optimized	48.98	852.52
Enhancement [%]	411	61.01

5.6 The Effect of The Stiffness of The Rear Bearing

Bearing preload is a key factor in governing the stiffness of the bearings which can be increased by changing the preload applied to it. This is applicable to an optimum level after which the stiffness of the bearing reduces with additional preload [106]. This section investigates the effects of increasing the rear bearing stiffness value in relation to the optimum location of the bearing.

The rear bearing stiffness value is increased by 10%, and the same analysis is repeated to investigate how the optimum location of the rear bearing location changes, as well as the value of the first natural frequency.

Table 13. The effect of the rear bearing stiffness on the optimum rear bearing location and the first natural frequency value.

Bearing stiffness [N/m]	Optimum rear bearing location [mm]	Frequency [Hz]
7.50+008	162	850.75
8.25+008	167	855.43
9.00+008	169	858.12
9.75+008	171	860.41

5.7 Application To a Real Case

The authors of [107] investigated the vibration resistance of CNC lathe machine tools in an operational production environment. Using impact testing, they measured the dynamic characteristics and frequency response functions of the spindle units on multiple machines. These results were compared to calculated dynamic properties from spindle assembly finite element models. The authors were able to estimate the actual bearing stiffness and preload

conditions in the machines by matching the experimental and simulated responses. Because the geometry of the analyzed spindle, as well as the stiffness values of the bearings, are available, it was used as a case study to apply the optimization introduced earlier in this chapter, as there is a reference experimental validation of the spindle system in [107]. Figure 36 illustrates the spindle unit described in [107].

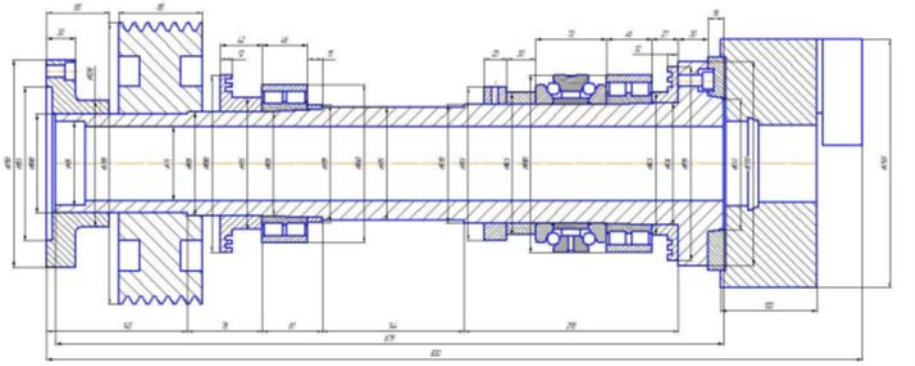

Figure 36. Spindle unit of machine tool.

The 3D geometry of the spindle unit was created using Figure 36. The remodeled geometry is illustrated in Figure 37.

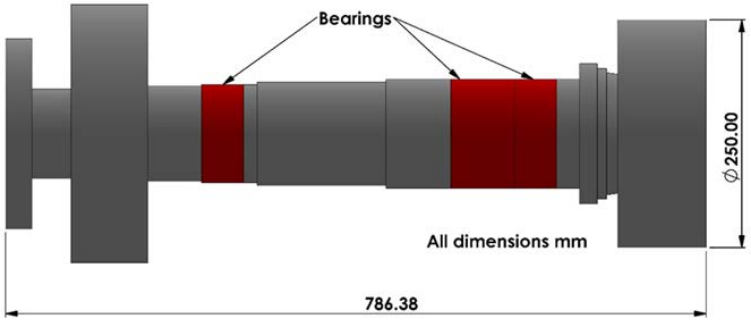

Figure 37. The remodeled geometry.

Figure 38 a) illustrates the results of the spindle unite impact testing in [107]. The blue curve is of interest because the values of the stiffness of the spindle bearings are available in [107]. Figure 38 b) shows the result of the modal finite element analysis of the remodeled spindle unite. As can be seen in Figure 31, the error in the first frequency value is 0.8%. The following settings are set for the analysis:

- The geometry in Figure 37 is used.

- Structural steel material is used with a density of 7.85e-06 kg/mm³, Young's Modulus of 2e+05 MPa, tensile yield strength of 250 MPa and a tensile ultimate strength of 460 MPa.
- For the connections, three bearings connections are used with the same exact locations shown in Figure 37. The connection type is Body-Ground and the value of the stiffness is set to match the values in [107]
- Mesh details: The mesh is generated using ANSYS V19, the elements are tetrahedral with a total element count of 129883 and a node count of 194976. The element size is 10 mm while the average surface area of the model is 17672 mm². Mesh quality was assessed using skewness. The skewness metric showed a minimum value of 2.800e-004, a maximum of 0.97437, an average of 0.23669, and a standard deviation of 0.13372

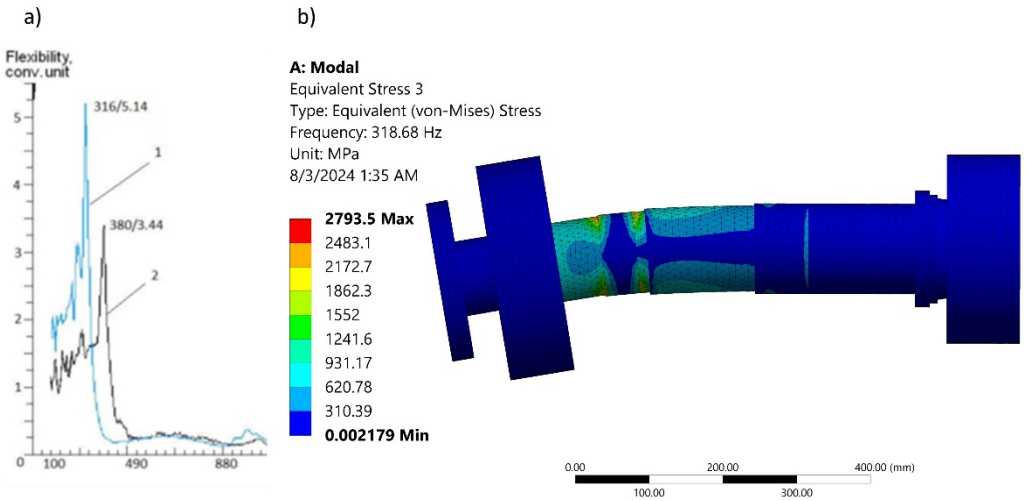

Figure 38. The results of the impact testing in [10], b) The modal analysis result of the remodeled spindle.

The mass of the mentioned system is 68.18 kg when only the spindle shaft and the chuck are considered. The thickness of the shaft of the equivalent spindle system is 13.5 mm after repeating the optimization process described in this chapter. The radius of the shaft next to the chuck is 96.41mm. The optimized rear bearing location is 216.48 mm measured from the free end of the shaft as illustrated in figure 39 b) while it was 243.53 mm in the model of [107].

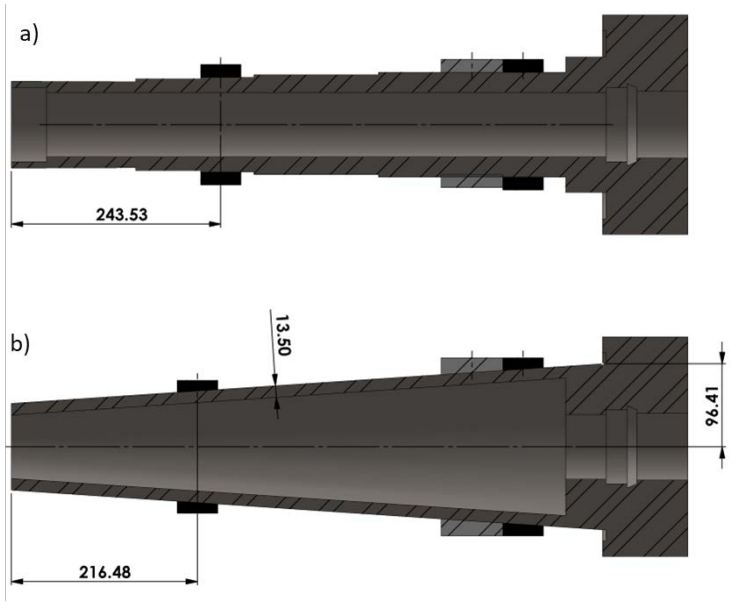

Figure 39. a) The remodeled spindle unite in [10], b) The optimized spindle unite.

Figure 40 a) illustrates the finite element method analysis of the model presented in [107], revealing that the first natural frequency value is 487.75 Hz, as well as the mode shape. Figure 40 b) illustrates the optimized finite element method analysis of the model, which reveals that the first natural frequency value is 561.63 Hz, along with the mode shape.

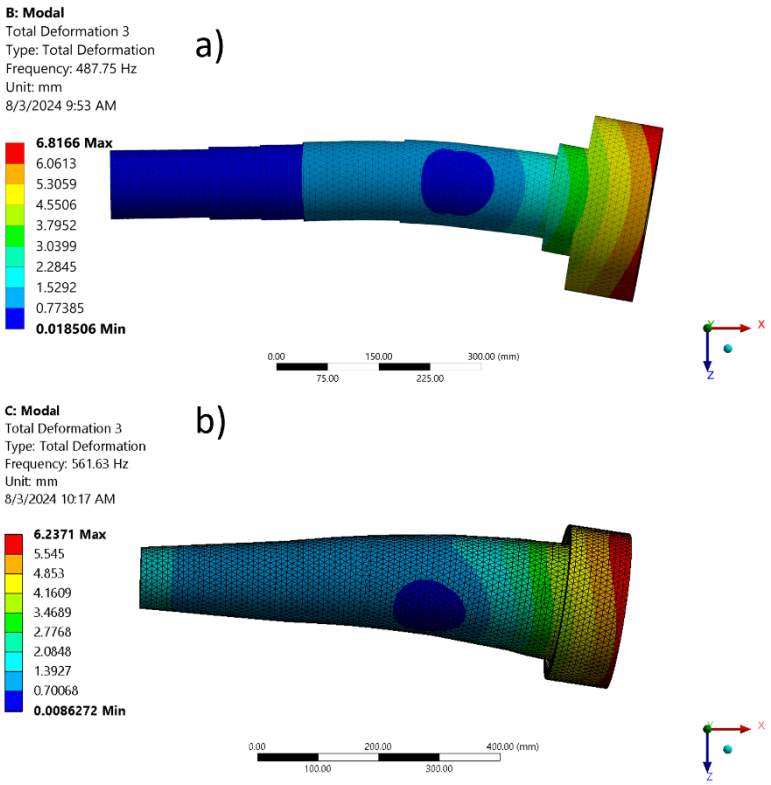

Figure 40. a) The modal analysis result of the remodeled spindle unite in [10], b) The modal analysis result of the optimized spindle unite.

The following settings are set for analyzing the model illustrated in figure 39 a):

- Structural steel material is used with a density of 7.85e-06 kg/mm³, Young's Modulus of 2e+05 MPa, tensile yield strength of 250 MPa and a tensile ultimate strength of 460 MPa.
- For the connections, three bearings connections are used with the same exact locations shown in Figure 38 a). The connection type is Body-Ground and the value of the stiffness is set to match the values in [107]
- Mesh details: The mesh is generated using ANSYS V19, the elements are tetrahedral with a total element count of 78181and a node count of 120608. The element size is 10 mm while the average surface area of the model is 15090 mm². Mesh quality was assessed using skewness. The skewness metric showed a minimum value of 3.5943e-004, a maximum of 0.90273, an average of 0.22441, and a standard deviation of 0.12874.

The following settings are set for analyzing the model illustrated in figure 39 b):

- Structural steel material is used with a density of 7.85e-06 kg/mm³, Young's Modulus of 2e+05 MPa, tensile yield strength of 250 MPa and a tensile ultimate strength of 460 MPa.
- For the connections, three bearings connections are used with the same exact locations shown in Figure 38 a). The connection type is Body-Ground and the value of the stiffness is set to match the values in [107]
- Mesh details: The mesh is generated using ANSYS V19, the elements are tetrahedral with a total element count of 87038and a node count of 136268. The element size is 10 mm while the average surface area of the model is 22944 mm². Mesh quality was assessed using skewness. The skewness metric showed a minimum value of 1.5789e-006, a maximum of 0.93099, an average of 0.2233, and a standard deviation of 0.12419.

As can be concluded from Figure 40, the optimized spindle model shows a 15% increase in the first natural frequency value over the spindle model proposed in [107].

Overall, the previous example demonstrates the effectiveness of the optimization process, including the optimization parameters and method used. These parameters and method can be applied to a variety of spindle systems.

5.7.1 Related Publications

Alzghoul Mohammad, Sarka Ferenc, Szabó Ferenc János (2023) Improving Chatter Performance of a Lathe Spindle through Grapho-Optimization. DESIGN OF MACHINES AND STRUCTURES: A PUBLICATION OF THE UNIVERSITY OF MISKOLC, 13: (2) pp. 5-12.

6 CONCLUSIONS

6.1 Introduction

This last chapter sums up the main findings, impacts, and future work from this research on optimizing lathe spindles to reduce chatter. The design changes explored show potential for better spindle performance through higher natural frequencies.

The overall findings will summarize the results of optimizing two structural parameters, the diameter of the shaft next to the chuck and the rear bearing position. These two parameters are selected given that the optimized spindle system will remain simple and maintain its overall mass. The importance of increasing natural frequency without changing total system mass will be highlighted.

The detailed findings will recap the modeling approach, beam theory used, specific parameters optimized, and the Kun-Tucker and Response Surface techniques used.

The future work section will outline suggested next steps for building on this research. Ideas include looking at variable bearing stiffness, trying different spindle designs, studying workpiece shape impacts, validating the results experimentally, and analyzing manufacturing costs. Possible broader uses and impacts will also be discussed.

In closing, the key contributions, limits, and future opportunities of this dissertation will be reviewed. The bigger picture potential of chatter reduction through spindle optimization will be shown. By thoroughly recapping the research, this concluding chapter will identify ways to further explore this important but understudied area of machine dynamics.

6.2 Overall findings

This study was aimed at enhancing the performance of a lathe spindle system in terms of chatter occurrence by implementing structural modifications to the spindle system while keeping its mass constant. These structural modifications involved altering the diameter of the spindle shaft near the chuck and adjusting the location of the rear bearing. The results indicate that the optimization of these two parameters can lead to an increase in the value of the first natural frequency and an enhancement in the stress capacity of the spindle system. Two optimization techniques were employed: Kuhn-Tacker optimization and the response surface methodology.

It was found that very similar results were obtained with both methods, suggesting that either technique can be effectively used with such a system.

6.3 Detailed Findings

As the primary objective of this research is to optimize a lathe machine spindle system with regard to chatter occurrence, the study pursued this goal by examining two well-known beam theories: Bernoulli beam theory and Timoshenko beam theory. Timoshenko beam theory was chosen because it aligns better with the objective of the research. Subsequently, two different optimization techniques were applied to compare both the results and the optimization methods themselves.

In turning, most research related to chatter primarily focuses on the cutting tool itself and the adjustment of cutting parameters to avoid chatter. Little attention is given to the structural modifications of the spindle system. This is why the topic of this research was chosen.

Furthermore, in the field of optimization methods for chatter in machining-related research, relatively complex techniques are often applied. For this reason, the Kuhn-Tucker method was chosen, owing to its simplicity and yet strong performance. Subsequently, the response surface methodology was employed to compare its outcomes with those achieved using the Kuhn-Tucker method.

Based on the findings of this study, greater emphasis should be placed on spindle system design in relation to chatter occurrence. This study demonstrates that chatter can be predicted, shifted up, and prevented by implementing structural modifications to the spindle system. Thus, addressing chatter is not solely reliant on adjusting cutting tools and parameters.

Furthermore, the optimization of such systems does not always require the use of complex methods, as demonstrated in this study through the application of the Kuhn-Tacker optimization method.

6.4 Future Studies

The study conducted in this research can be further developed, and other parameters can be investigated. Below are some ideas on how to expand this research:

1. Since this study assumes a constant bearing stiffness, it would be intriguing to conduct a similar study while considering varying bearing stiffness. This variability in bearing

stiffness could result from what is known as 'parametric excitation' within the bearing system.

2. The mass of the chuck significantly contributes to the overall mass of the spindle system. It would be intriguing to explore how altering both the mass and geometry of the chuck impacts the performance of the spindle system, particularly in terms of mitigating chatter occurrence. Investigating whether the mass and geometry of the chuck can be optimized is particularly relevant, given its role in securely holding the workpiece.
3. Investigating the energy consumption difference between the optimized and non-optimized spindle systems. By quantifying how much energy each system requires, insights can be gained into the efficiency gains or losses resulting through optimization. This analysis will not only contribute to a more comprehensive understanding of the performance improvements but also has practical implications for energy-efficient machining processes
4. Conducting a manufacturing cost analysis and investigating whether the additional manufacturing cost of the optimized spindle system is justified by the improvements in chatter performance and stress capacity.
5. An interesting optimization case would involve reducing the mass of the same non-optimized spindle system while maintaining its first natural frequency at the same value.
6. Investigating the effect of the geometry of the workpiece on the spindle system in terms of the first natural frequency of the spindle system.
7. Analyzing both the non-optimized and optimized models to obtain additional results, including but not limited to higher modes, critical speeds, stress levels, and deflection responses under various loading scenarios.
8. Investigating the differences in optimal cutting parameters between the non-optimized and optimized models and how these differences affect the productivity of the cutting tools, tool life, and machining time.
9. Investigating the possibility of achieving equivalent performance in terms of chatter occurrence while maintaining the same overall mass of the spindle system by employing a stepped shaft design instead of a truncated hollow cone-shaped shaft.
10. Conducting the same study with various types of bearings, each having different stiffness values.

11. Validating the results of the first natural frequency and the stress of the optimized spindle system experimentally.
12. Assessing the cost increase associated with the larger bearings of the optimized spindle system compared to the non-optimized system and investigating whether this rise in bearing costs justifies the improvements in the optimized spindle system regarding chatter occurrence.

In conclusion, this thesis demonstrates the potential of spindle optimization as a technique for chatter reduction, complementing conventional cutting parameter adjustment. The geometry and bearing modifications explored show the concept of increased frequency response through dynamics-based enhancements. These initial findings open the door for improved understanding and design of spindle systems to withstand detrimental vibrations. This research marks an important first step toward unlocking the full performance potential of lathe spindle systems, paving the way for continued exploration in this impactful area of manufacturing.

7 THESES

7.1 Thesis One

I proved that transforming the geometry of a horizontal lathe machine spindle shaft from a uniform to a conical shape—increasing its diameter towards the chuck and reducing its thickness—significantly improves the vibrational performance of the spindle system. This modification, achieved while maintaining the overall mass and length of the spindle constant. The result is a notable enhancement in the natural frequency of the spindle system, leading to a reduced likelihood of machining chatter and indicating superior stability and precision in machining operations.

Related publications: **MA1, MA2 and M4**

7.2 Thesis Two

I proved that strategic optimization of the rear bearing location within a horizontal lathe machine spindle system plays a significant role in enhancing its vibrational characteristics. Through the finite element method, this optimization was identified as a pivotal factor in improving the natural frequency of the spindle, thereby bolstering its resistance to machining chatter. This consideration, in conjunction with the geometric modifications to the spindle shaft, highlights a comprehensive approach to improving the dynamic performance of machining equipment.

Related publications: **MA1 and MA2**

7.3 Thesis Three

I proved that, within a horizontal lathe machine spindle system, there exists a direct positive correlation between the stiffness of the rear bearing and the first natural frequency of the spindle system. Additionally, the stiffness of the rear bearing influences its optimum placement for achieving the highest possible first natural frequency of the spindle system. This discovery unveils the intricate interplay between bearing stiffness and its positioning, shedding light on a crucial aspect of spindle design that directly impacts machining stability and efficiency. By optimizing both the stiffness and the location of the rear bearing, this research contributes a significant advancement towards refining spindle systems for enhanced performance.

Related publications: **MA1**

7.4 Thesis Four

The derived expression for calculating the natural frequencies and plotting the mode shapes of a simply-supported beam with an overhang mass, validated by finite element analysis, allows for optimizing the point mass and support location without requiring complex analysis. This approach significantly enhances the performance of systems such as machine tool spindles and boring bars by providing a more efficient method for determining their dynamic characteristics.

Related publications: **MA5**

8 REFERENCES

[1] C. L. Lida Zhu, "Recent progress of chatter prediction, detection and suppression in milling," *Mechanical Systems and Signal Processing,* vol. 143, 2020.

[2] M. W. W.-H. Z. Y. Y. Xue-Bin Qin, "Chatter suppression with productivity improvement by scheduling a C3 continuous feedrate to match spindle speed variation," *Mechanical Systems and Signal Processing,* vol. 188, 2023.

[3] B. Stone, Chatter and Machine Tools, Perth: Springer, 2014.

[4] A. Yadav, D. Talaviya, A. Bansal and M. Law, "Design of Chatter-Resistant Damped Boring Bars Using a Receptance Coupling Approach," *Journal of Manufacturing and Materials Processing,* vol. 4, pp. 53-79, 2020.

[5] H. Aguiar, A. Hassui, D. Suyama and A. Magri, "Reduction of internal turning surface roughness by using particle damping aided by airflo," *The International Journal of Advanced Manufacturing Technology,* vol. 106, 2020.

[6] G. P. P. S. M. J. G. M. S. P. E. Lawrance, "Prediction of cutting performance using artificial neural network during buffered impact damper-assisted boring process," *Multiscale and Multidisciplinary Modeling, Experiments and Design,* vol. 4, no. 4, pp. 671-684, 2023.

[7] V.-C. Tong, J. Hwang, J. Shim, J.-S. Oh and S.-W. Hong, "Multi-objective Optimization of Machine Tool Spindle-Bearing System," *International Journal of Precision Engineering and Manufacturing,* vol. 21, no. 10, pp. 1885-1902, 2020.

[8] J. a. S. T. a. S. P. Chrzanowski, "Spindle Error Movements and Their Measurement," *Applied Sciences,* vol. 11, 2021.

[9] C.-W. Lin, "Optimization of Bearing Locations for Maximizing First Mode Natural Frequency of Motorized Spindle-Bearing Systems Using a Genetic Algorithm," *Applied Mathematics,* vol. 5, no. 14, pp. 2137-2152, 2014.

[10] C. L. Qian Yi, Q. Ji, D. Zhu, Y. Jin and L. Li., "Design optimization of lathe spindle system for optimum energy efficiency," *Journal of Cleaner Production,* vol. 250, 2020.

[11] A. M. K. Marian Wiercigroch, "Frictional chatter in orthogonal metal cutting," *Philos. Trans. Royal Soc. London Ser. A: Mathematical Phys. Eng. Sci.,* vol. 359, pp. 713-738, 2001.

[12] T. J. B. Matthew A. Davies, "Thermomechanical Oscillations in Material Flow During High-Speed Machining," *Philos. Trans. Royal Soc. London Ser. A: Mathematical Phys. Eng. Sci,* vol. 359, no. 1781, pp. 821-846, 2001.

[13] B. Z. L. Yan, "Research on milling stability of thin-walled parts based on improved multi-frequency solution," *he International Journal of Advanced Manufacturing Technology,* vol. 102, no. 1, p. 431–441, 2019.

[14] R. N. Arnold, "Cutting Tools Research: Report of Subcommittee on Carbide Tools: The Mechanism of Tool Vibration in the Cutting of Steel," *Proceedings of the Institution of Mechanical Engineers,* vol. 154, no. 1, p. 261–284, 1964.

[15] D. M. Z. C. Zhehe Yao, "On-line chatter detection and identification based on wavelet and support vector machine," *Journal of Materials Processing Technology,* vol. 210, no. 5, pp. 713-719, 2010.

[16] S. S. Ö. T. C.S. Anderson, "A passive adaptor to enhance chatter stability for end mills," *International Journal of Machine Tools and Manufacture,* vol. 47, no. 11, pp. 1777-1785, 2007.

[17] M. F. I. G. X. S. R. U.-E. J. H. J. Albizuri, "An active system of reduction of vibrations in a centerless grinding machine using piezoelectric actuators,," *International Journal of Machine Tools and Manufacture,,* vol. 47, no. 10, pp. 1607-1614, 2007.

[18] J. P. L. T. D. H. N. S. M. R. C.-M. K. R. X. B. W. K. B. Jeffrey L. Dohner, "Mitigation of chatter instabilities in milling by active structural control,," *Journal of Sound and Vibration,,* vol. 269, no. 1-2, pp. 197-211, 2004.

[19] M. a. K. C. R. Chen, "Control Approaches to the Suppression of Machining Chatter Using Active Magnetic Bearings," *IEEE Transactions on Control Systems Technology,* vol. 15, no. 2, pp. 220-232, 2007.

[20] K. C. Dan Wu, "Chatter suppression in fast tool servo-assisted turning by spindle speed variation,," *International Journal of Machine Tools and Manufacture,,* vol. 50, no. 12, pp. 1038-1047, 2010.

[21] G. R. Andreas Otto, "Application of spindle speed variation for chatter suppression in turning,," *CIRP Journal of Manufacturing Science and Technology,,* vol. 6, no. 2, pp. 102-109, 2013.

[22] H. M. G. V. M. R. M. Kambiz Haji Hajikolaei, "Spindle speed variation and adaptive force regulation to suppress regenerative chatter in the turning process,," *Journal of Manufacturing Processes,,* vol. 12, no. 2, pp. 106-115, 2010.

[23] J. M. Y. A. Y. Yang, "Optimization of multiple tuned mass dampers to suppress machine tool chatter,," *International Journal of Machine Tools and Manufacture,,* vol. 50, no. 9, pp. 834-842, 2010.

[24] S.A.Tobias, "Machine tool vibration research," *International Journal of Machine Tool Design and Research,* vol. 1, no. 1-2, pp. 1-14, 1961.

[25] E. B. Marian Wiercigroch, "Sources of nonlinearities, chatter generation and suppression in metal cutting," *philosophicaltransactions:Mathematical, Physical andEngineeringSciences,* vol. 359, p. 663–693, 2001.

[26] K. A. Y. Mohammadi, "Frequency domain analysis of regenerative chatter in machine tools with Linear Time Periodic dynamics,," *Mechanical Systems and Signal Processing,,* vol. 120, pp. 378-391, 2019.

[27] E. T. G. S. M. Kuljanić, "Vibrations and Chatter in Machining: State of the Art and New Approaches," in *Advanced Manufacturing Systems and Technology - AMST'08*, Udine, 2008.

[28] K. L. M. Großmann, "Synthesis of Stability Lobe Diagrams," in *Process Machine Interactions*, Berlin, Heidelberg, 2013.

[29] M. S. R.Paurobally, "A review of chatter vibration research in turning," *International Journal of Machine Tools & Manufacture,* vol. 61, pp. 27-47, 2012.

[30] K. Y. K. M. R. T. a. K. S. Agus Susanto, "Vibration Analysis in Milling of Thin-Walled Workpieces Using Hilbert–Huang Transform," in *Proceedings of International Conference on Leading Edge Manufacturing in 21st century : LEM21*, 2017.

[31] N. H. T. S. A. Hanna, "A Theory of Nonlinear Regenerative Chatter," *Journal of Engineering for Industry,* vol. 96, no. 1, pp. 247-255, 1974.

[32] K. S. K. Y. N. Suzuki, "Effect of cross transfer function on chatter stability in plunge cutting," *Journal of Advanced Mechanical Design, Systems, and Manufacturing,* vol. 4, p. 883–891, 2010.

[33] D. B. R. E. G. S. Z. Dombovari, "On the global dynamics ofchatter in the orthogonal cutting model," *International Journal of Non-Linear Mechanics,* vol. 46, p. 330–338, 2011.

[34] T. P. N.K. Chandiramani, "Dynamics of 2-dof regenerative chatter during turning," *Journal of Sound and Vibration,* vol. 290, p. 448–464, 2006.

[35] Y. T. C.K. Chen, "Astability analysis of turning a tailstock supported flexible work-piece," *International Journal of Machine Tools and Manufacture ,* vol. 46, pp. 18-25, 2006.

[36] Y. T. C.K. Chen, "Astability analysis of regenerative chatter in turning process without using tail stock," *The International Journal of Advanced Manufacturing Technology,* vol. 29, p. 648–654, 2006.

[37] C. A.V. Dassanayake, "On nonlinear cutting response and tool chatter in turning operation," *Communications in Nonlinear Science and Numerical Simulation,* vol. 13, p. 979–1001, 2008.

[38] Y. A. M. Eynian, "Chatter stability of general turning operations with process damping," *Journal of Manufacturing Science and Engineering,* vol. 131, p. 41005–41010, 2009.

[39] A. a. M. D. Bhatnagar, "Visualization of Frequency Response Using Nyquist Plots,," *SAE Technical Paper,* p. 8, 2022.

[40] A. F. L. F. M. Buscarino, "Nyquist plots under frequency transformations," *Systems & Control Letters,* vol. 125, pp. 16-21, 2019.

[41] S. O. S. N. S. Y. E. Turkes, "Linear analysis of chatter vibration and stability for orthogonal cutting in turning," *International Journal of Refractory Metals and Hard Materials,* vol. 29, pp. 163-169, 2011.

[42] H.E.Meritt, "Theory of self-excited machine–tool chatter," *Transactions of the ASME Journal of Engineering for Industry,* vol. 87, p. 447–454, 1965.

[43] M.M.Nigm, "Amethod for the analysis of machine tool chatter," *International Journal of Machine Tool Design and Research,* vol. 21, p. 251–261, 1981.

[44] E. M. I. P. I.E. Minis, "Improved methods for the prediction of chatter inturning, Part 3. A generalized linear theory," *Journal of Engineering for Industry, Transactions ASME,* vol. 112, p. 28–35, 1991.

[45] W. C. Z.C. Wang, "Stability analysis of spinning stepped-shaft workpieces in a turning process," *Journal of Sound and Vibration,* vol. 250, p. 356–367, 2002.

[46] M. E. H. O. Y. Altintas, "Identification of dynamic cutting force coefficients and chatter stability with process damping," *CIRP Annals—Manufacturing Technology,* vol. 57, p. 371–374, 2008.

[47] L. L. d. L. F. C. A. A. E. G. Urbikain, "Stability prediction in straight turning of a flexible workpiece by collocation method," *International Journal of MachineTools and Manufacture,* Vols. 54-55, p. 73–81, 2012.

[48] F. K. W. P. F. C. Brecher, "Methodology for coupling a FEA-based process model with a flexible multi-body simulation of a machine tool," *CIRP International Workshop on Modeling of Machining Operations,* vol. 10, pp. 453-460, 2007.

[49] R. Mahdavinejad, "Finite element analysis of machine and workpiece instability in turning," *International Journal of Machine Tools and Manufacture,* vol. 45, p. 753–760, 2005.

[50] K. E. R. J .R. Baker, "Use of finite element structural models in analyzing machine tool chatter," *Finite Elements in Analysis and Design,* vol. 38, p. 1029–1046, 2002.

[51] J. N. C. K. Airao, "Finite element modeling of ultrasonic assisted turning with external heating," *Procedia CIRP,* vol. 102, pp. 64-66, 2021.

[52] Z. Yao, D. Mei and Z. Chen, "On-line chatter detection and identification based on wavelet and support vector," *J. Mater. Process. Technol,* vol. 210, p. 713–719, 2010.

[53] S. Yamato, T. Hirano, Y. Yamada, R. Koike and Y. Kakinuma, "Sensor-less on-line chatter detection in turning," *Precis. Eng,* vol. 51, p. 103–116, 2018.

[54] F. Khasawneh and E. Munch, "Chatter detection in turning using persistent homology," *Mech. Syst. Signal Process,* vol. 70, p. 527–541, 2016.

[55] F. Khasawneh, E. Munch and J. Perea, "Chatter Classification in Turning using Machine Learning and," *IFAC-PapersOnLine,* vol. 51, p. 195–200., 2018.

[56] I. Tansel, "Modelling 3-D cutting dynamics with neural networks," *Int. J. Mach. ToolsManuf,* vol. 32, p. 829–853, 1992.

[57] H. Cherukuri, E. Perez-Bernabeu, M. Selles and T. Schmitz, "A neural network approach for chatter prediction," *Procedia Manuf,* vol. 34, p. 885–892, 2019.

[58] S. Kumar and B. Singh, "Prediction of tool chatter in turning using RSM and ANN," *Mater. Today Proc,* vol. 5, p. 23806–23815, 2018.

[59] Y. Shrivastava, B. Singh and A. Sharma, "Identification of Chatter in Turning Operation using WD and EMD," *Mater. Today Proc,* vol. 5, p. 23917–23926, 2018.

[60] S. Kim and K. Ahmadi, "Estimation of vibration stability in turning using operational modal analysis," *Mech. Syst.,* vol. 130, p. 315–332, 2019.

[61] Y. Liu, T.-X. Li, K. Liu and Y.-M. Zhang, "Chatter reliability prediction of turning process system with," *Mech. Syst. Signal Process,* vol. 66, p. 232–247, 2016.

[62] X. Huang, M. Hu, Y. Zhang and C. Lv, "Probabilistic analysis of chatter stability in turning," *Int. J. Adv. Manuf. Technol,* vol. 87, p. 3225–3232, 2016.

[63] A. Cortadi, I. Irigoien, F. Boto, B. Sierra, A. Suarez and D. Galar, "A statistical data-based approach to instability detection and wear prediction in radial turning processes.," *Ekspolatacja Niezawodn. Maint. Reliab,* vol. 20, p. 405–412, 2018.

[64] A.-H. Tian, C.-B. Fu, X.-Y. Su and H.-T. Yau, " Lathe tool chatter vibration diagnostic using general regression neural network based on Chua's circuit and fractional-order Lorenz master/slave chaotic system," *J. Low Freq. Noise Vib. Act,* vol. 38, p. 953–966, 2018.

[65] T. Inamura and T. Sata, "Stability analysis of cutting under varying spindle speed," *CIRP Ann,* vol. 23, p. 119–120, 1974.

[66] T. Takemura, T. Kitamura, T. Hoshi and K. Okushimo, " Active suppression of chatter by programmed variation of spindle speed," *CIRP Ann,* vol. 12, p. 121–122, 1974, 23, 121–122.

[67] J. Sexton, R. Milne and B. Stone, "A stability analysis of single-point machining with varying spindle speed," *Appl. Math. Model. ,* vol. 1, p. 310–318, 1977.

[68] T. Hoshi, N. Sakisaka, I. Moriyama and M. Sato, "Study for practical application of fluctuating speed cutting for regenerative chatter control," *CIRP Ann,* vol. 25, p. 175–179, 1977.

[69] T. Tsao, M. McCarthy and S. Kapoor, " A New Approach to Stability Analysis of Variable Speed Machining Systems," *Int. J. Mach. Tools Manuf ,* vol. 33, p. 791–808, 1933.

[70] E. Soliman and F. Ismail, " Chatter Suppression by Adaptive Speed Modulation Int.," *J. Mach. Tools Manuf,* vol. 37, p. 355–369, 1977.

[71] S. Jayaram, S. Kapoor and R. DeVor, "Analytical stability analysis of variable spindle speed machining," *J. Manuf. Sci. Eng.,* vol. 122, p. 391–397, 2000.

[72] E. Al-Regib, J. Ni and S.-H. Lee, "Programming spindle speed variation for machine tool chatter suppression.," *Int. J. Mach. Tools Manuf,* vol. 43, p. 1229–1240, 2003.

[73] H. Zhang, M. Jackson and J. Ni, "Spindle speed variation method for regenerative machining chatter control," *Int. J. Nanomanuf,* vol. 3, p. 73–99, 2009.

[74] M. Zatarain, I. Bediaga, J. Muñoa and R. Lizarralde, "Stability of milling processes with continuous spindle speed variation: Analysis in the frequency and time domains, and experimental correlation," *CIRP Ann,* vol. 57, p. 379–384, 2008.

[75] D. Barrenetxea, J. Marquinez, I. Bediaga and L. Uriarte, "Continuous workpiece speed variation (CWSV): Model based practical application to avoid chatter in grinding.," *CIRP Ann,* vol. 58, p. 319–322, 2009.

[76] T. Insperger and G. Stepan, Semi-Discretization for Time-Delay Systems: Stability and Engineering Applications, London: Springer New York, NY, 2010.

[77] D. Wu, K. Chen and X. Wang, " An investigation of practical application of variable spindle speed machining to noncircular turning process," *Int. J. Adv. Manuf. Technol,* vol. 44, p. 1094–1105, 2009.

[78] D. Wu and K. Chen, " Chatter suppression in fast tool servo-assisted turning by spindle speed variation," *Int. J. Mach. Tools Manuf ,* vol. 50, p. 1038–1047, 2010.

[79] A. Yilmaz, E. Al Regib and J. Ni, "Machine Tool Chatter Suppression by Multi Level Random Spindle Speed Variation," *J. Manuf. Sci. Eng,* vol. 124, p. 208–216, 2002.

[80] A. Otto and G. Radons, "Application of spindle speed variation for chatter suppression in turning," *CIRP J. Manuf. Sci. Technol,* vol. 6, p. 102–109, 2013 .

[81] G. Urbikain, D. Olvera, L. De Lacalle and A. Elías-Zúñiga, "Spindle speed variation technique in turning operations: Modeling and real implementation," *J. Sound Vib,* vol. 383, p. 384–396, 2016.

[82] F. Yang, B. Zhang and J. Yu, "Chatter suppression with multiple time-varying parameters in turning," *J. Mater. Process. Technol,* vol. 141, p. 431–438, 2003.

[83] K. JAUHARI, "Vibration reduction of spindle-bearing system by design optimization," *WSEAS TRANSACTIONS on APPLIED and THEORETICAL MECHANICS,* pp. 85-91, 2018.

[84] Y. a. L. C. a. T. Y. a. C. X. a. Z. X. Lv, "Towards Lightweight Spindle of CNC Lathe Using Structural Optimization Design for Energy Saving," *IEEE 16th International Conference on Automation Science and Engineering (CASE),* pp. 220-225, 2020.

[85] V. H. J. S. J. e. a. Tong, "Multi-objective Optimization of Machine Tool Spindle-Bearing System," *Int. J. Precis. Eng. Manuf.,* vol. 21, no. 10, p. 1885–1902, 2020.

[86] Timoshenko, Stephen P., "The Strength of Materials in the Seventeenth Century," in *History of strength of Materials*, vol. 1, New York, Dover Publication, INC., New York, 1983, pp. 7-40.

[87] S. S. Rao, Vibration of continuous systems, Hoboken, New Jersey: John Wiley & Sons, Inc., 2007, p. 720.

[88] O. A. Bauchau and J. I. Craig, "Euler-Bernoulli beam theory," in *Structural Analysis*, vol. 163, O. A. Bauchau and J. I. Craig, Eds., Dordrecht, Springer Netherlands, 2009, pp. 173-221.

[89] S. S. Rao, Mechanical Vibrations, Upper Saddle River: Pearson, 2011.

[90] A. Labuschagne, N. F. J. Van Rensburg and A. J. van der Merwe, "Comparison of linear beam theories," *Mathematical and Computer Modelling,* vol. 49, no. 1-2, pp. 20-30, 2009.

[91] A. M. Ahmed and A. M. Rifai, "Euler-Bernoulli and Timoshenko Beam Theories Analytical and Numerical Comprehensive Revision," *European Journal of Engineering and Technology Research2021,* vol. 6, no. 7, pp. 20-32, 2021.

[92] P. Laura, J. Pombo and E. Susemihl, "A note on the vibrations of a clamped-free beam with a mass at the free end," *Journal of Sound and Vibration,* vol. 37, no. 2, pp. 161-168, 1974.

[93] J. Hong, J. Dodson, S. Laflamme and A. Downey, "Transverse Vibration of Clamped-Pinned-Free Beam with Mass at Free End," *Applied Sciences,* vol. 9, no. 15, pp. 2996-3012, 2019.

[94] S. C. A. S. Mohammad Alzghoul, "Dynamic modeling of a simply supported beam with an overhang mass," *Pollack Periodica,* vol. 14, no. 2, p. 42–47, 04 May 2022.

[95] A. P. B. J. S. o. c. P. 1. t. a. r. d. R J Lambert, "Some characteristics of rolling-element bearings under," *Proceedings of the Institution of Mechanical Engineers, Part K: Journal of Multi-body Dynamics,* vol. 220, no. 3, pp. 157-170, 2006.

[96] S. B. Potter SJ, "The calculation of the response of spindle-bearing systems to oscillating forces.," MTIRA research report, 1974.

[97] S. BJ, "The receptances of beams, in closed form, including the effects of shear and rotary inertia.," *Proc IMechE,* vol. 206, no. 2, pp. 87-94, 1992.

[98] Z. Árpád, Gépelemek I, Budapest: Nemzeti Tankönyvkiadó, 1999.

[99] [Online]. Available: https://www.haas.co.uk/lathes/st-35l/. [Accessed 20 04 2023].

[100] F. F. Ehrich, Handbook of Rotordynamics, McGraw-Hill, 1992.

[101] D. C. Montgomery, Design and Analysis of Experiments, John Wiley & Sons, 217.

[102] D. C. M. C. M. A.-C. RAYMOND H. MYERS, Response surface methodology: process and product optimization using designed experiments, John Wiley & Sons, 2016.

[103] B. İ. H. Bas Deniz, "Modeling and optimization I: Usability of response surface methodology," *ournal of Food Engineering,* vol. 78, no. 3, pp. 836-845, 2007.

[104] A. I. M. S. Khuri, "Response surface methodology," *WIREs Computational Statistics,* vol. 2, no. 2, pp. 128-149, 2010.

[105] S. C. Richard Leach, Precision Metal Additive Manufacturing, Boca Raton: CRC Press, 2020.

[106] T. Harris and M. Kotzalas, "Essential Concepts of Bearing Technology," in *Rolling Bearing Analysis*, New Yourk, Taylor & Francis Group, 2006, pp. 119-128.

[107] F. S. a. N. K. a. S. Shemyakin, "Operational Assessment of Machine Tool Vibration Resistance," *Procedia Engineering,* vol. 150, pp. 215-219, 2016.

[108] J. C. Guillem Quintana, "Chatter in machining processes: A review," *International Journal of Machine Tools and Manufacture,* vol. 51, no. 5, pp. 363-376, 2011.

[109] M. M. K. Jasiewicz, "Implementation of an Algorithm to Prevent Chatter Vibration in a CNC System," *Materials,* vol. 12, 2019.

[110] "Manufacturing Automation Laboratories," [Online]. Available: https://www.malinc.com/. [Accessed 3 09 2022].

[111] "MetalMax, Manufacturing Laboratories Inc," [Online]. Available: https://www.mfg-labs.com/. [Accessed 03 09 2022].

[112] G. a. A. A. a. L. d. L. L. N. a. A. M. a. A. M. A. a. V. F. Urbikain, "A Reliable Turning Process by the Early Use of a Deep Simulation Model at Several Manufacturing Stages," *Machines,* vol. 5, p. 15, 2017.

9 LIST OF PUBLICATIONS RELATED TO THE TOPIC OF THE RESEARCH FIELD

MA1. Mohammed, Alzghoul; Sarka, Ferenc; Szabó, Ferenc János, Optimization of spindle system first natural frequency values using response surface methodology of variance, VOSTOCHNO-EVROPEISKII ZHURNAL PEREDOVYKH TEKHNOLOGII / EASTERN- EUROPEANJOURNAL OF ENTERPRISE TECHNOLOGIES1 : 1pp. 17-25. , 9 p. (2025).
DOI: https://doi.org/10.15587/1729-4061.2025.320497

MA2. Alzghoul, Mohammad; Sarka, Ferenc; Szabó, Ferenc János, Improving Chatter Performance of a Lathe Spindle through Grapho-Optimization, DESIGN OF MACHINES AND STRUCTURES13 : 2pp. 5-12. , 8 p. (2023)
DOI: https://doi.org/10.32972/dms.2023.012

MA3. Alzghoul, Mohammad; Sarka, Ferenc; Szabó, Ferenc J.,Analytical and Experimental Techniques for Chatter Prediction, Suppression and Avoidance in Turning: Literature Survey, DESIGN OF MACHINES AND STRUCTURES12 : 2pp. 33-43. , 11 p. (2022)
DOI: https://doi.org/10.32972/dms.2022.011

MA4. Alzghoul, Mohammad; Sarka, Ferenc; Szabó, Ferenc J., A Spindle System Analysis Using Systems Receptance Coupling Approach, DESIGN OF MACHINES AND STRUCTURES12 : 2pp. 25-32. , 8 p. (2022)
DOI: https://doi.org/10.32972/dms.2022.010

MA5. Alzghoul, Mohammad; Cabezas, Sebastian; Szilágyi, Attila, Dynamic modeling of a simply supported beam with an overhang mass, POLLACK PERIODICA: AN INTERNATIONAL JOURNAL FOR ENGINEERING AND INFORMATIONSCIENCES17 : 2pp. 42-47. , 7 p. (2022)
DOI: https://doi.org/10.1556/606.2022.00523

MA6. Al-zgoul, Mohammad; Szilágyi, Attila, DYNAMICAL SIMULATION OF A CNC TURNING CENTER,DESIGN OF MACHINES AND STRUCTURES10 : 2pp. 91-96. , 6 p. (2020)
DOI: https://doi.org/10.32972/dms.2020.019

MA7. Al-zgoul, Mohammad; Szilágyi, Attila, DYNAMICAL SIMULATION OF A CNC TURNING CENTER (SURVEY PAPER). DESIGN OF MACHINES AND STRUCTURES10 : 2pp. 85-90. , 6 p. (2020)
DOI: https://doi.org/10.32972/dms.2020.018

10APPENDICES

Appendix A: Equation (5.8) derivation

This appendix shows the derivation of equation 5.8 which obtains the relationship between the axial location and the diameter associated with it along the conical shaft The figure below illustrates the case.

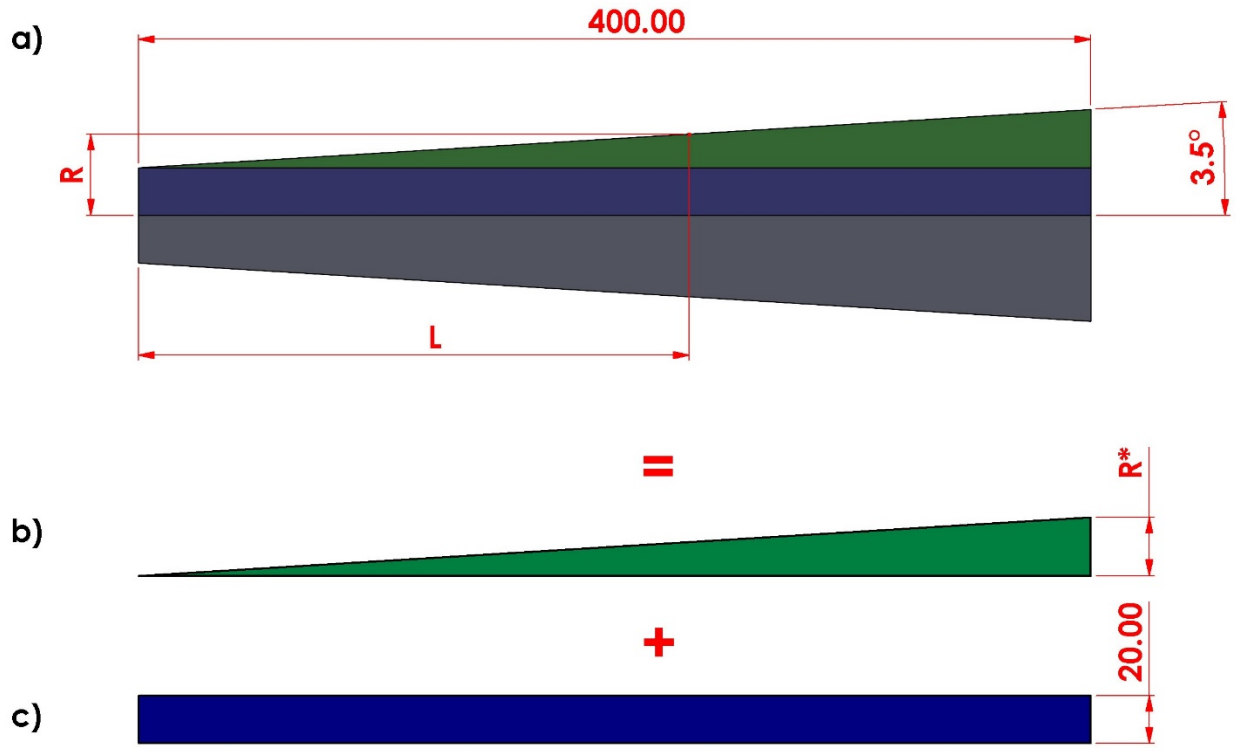

Figure 41. a) projection view of the shaft, b) sub-system 1, c) sub-system 2.

Given that the angle of the cone is a fixed value, the tangent relation can be utilized.

$$Tan\ 3.5 = \frac{L}{R^*} \xrightarrow{yields} R^* = 0.0612 * L$$

Then:

$$R = R^* + 20 \xrightarrow{yields} R = 0.0612L + 20$$

Appendix B: formulas of $\eta, \zeta, s, r, F_1, F_2, F_3, F_4, F_5, F_6$ and Δ

$$\eta = ([-\rho I w^2\left(1+\frac{E}{\lambda G}\right)+\sqrt{\rho I w^2\left(\rho I w^2\left(1-\frac{E}{\lambda G}\right)^2+4EA\right)}]/2EI)^{1/2}$$

$$\zeta = ([\rho I w^2\left(1+\frac{E}{\lambda G}\right)+\sqrt{\rho I w^2\left(\rho I w^2\left(1-\frac{E}{\lambda G}\right)^2+4EA\right)}]/2EI)^{1/2}$$

$$S = \frac{\rho w^2}{\lambda G\zeta} - \zeta$$

$$r = \frac{\rho w^2}{\lambda G\eta} - \eta w$$

$$F_1 = \sin\zeta L \sinh\eta L$$

$$F_2 = \cos\zeta L \cosh\eta L$$

$$F_3 = \cos\zeta L \cosh\eta L - 1$$

$$F_4 = \sin\zeta L \cosh\eta L$$

$$F_5 = \cos\zeta L \sinh\eta L$$

$$F_6 = \cos\zeta L - \cosh\eta L$$

$$\Delta = (2 - 2cos\zeta L\cosh\eta L + \left(\frac{r\eta^2}{s\zeta^2}-\frac{s\zeta^2}{r\eta^2}\right)\sin\zeta L\sinh\eta L = \rho w^2 A\left(2-2F_2+\left(\frac{r\eta^2}{s\zeta^2}-\frac{s\zeta^2}{r\eta^2}\right)F_1\right)$$